Activity-dependent regulation of synaptic neurotransmission by Ca2+ and tomosyn

Mancini, R.

2020

document version
Publisher's PDF, also known as Version of record

CHAPTER 3

Characterisation of spontaneous Ca^{2+} events and correlation to quantal release in primary neurons

Authors:
Roberta Mancini[1], Quentin Bourgeois Jaarsma[1], Rizky Lasabuda[1], Yong Qian[2], Robert E. Campbell[2] and Alexander J. Groffen[1,3]

Affiliations:
[1] Department of Functional Genomics, Faculty of Science, Center for Neurogenomics and Cognitive Research, Vrije Universiteit, De Boelelaan 1085, 1081HV Amsterdam, The Netherlands.
[2] Dept. of Chemistry, University of Alberta, Canada.
[3] Department of Clinical Genetics, Center for Neurogenomics and Cognitive Research, VU Medical Center, Amsterdam, The Netherlands.

Abstract

Ca^{2+} is an important signalling molecule which is critical for evoked neurotransmission and regulates spontaneous release. Resting neurons exhibit spontaneous local Ca^{2+} fluctuations, but their relation to quantal release events is uncertain. Here we apply two independent approaches to directly asses the role of Ca^{2+} in spontaneous release. First, we measured miniature excitatory postsynaptic currents (mEPSCs) and spontaneous Ca^{2+} events (SCEs) simultaneously in the same neuron using the Ca^{2+} indicator GCaMP6f, targeted to synaptic vesicles using synaptophysin-1. Although high extracellular Ca^{2+} increased the number of SCEs and mEPSCs, no strict temporal correlation connecting the two events was found. Second, we developed a new fluorescent probe sypHyJRex which can detect Ca^{2+} signals and secretion events for the same synaptic vesicle. Preliminary sypHyJRex data showed that spontaneous Ca^{2+} events co-occurred with spontaneous vesicle fusion events in the same synapse. This evidence adds validity to the hypothesis that SCEs may trigger spontaneous vesicle release events. However, the lack of a strict correlation with mEPSCs suggests that these events may contribute only to a small fraction of the overall spontaneous release events, or involve non-glutamatergic vesicles. Further studies are required to unravel the molecular mechanism linking spontaneous vesicle release and SCEs.

Introduction

Neuronal Ca^{2+} ions

Ca^{2+} ions are among the most versatile messengers that control many pathways in all cell types. They regulate gene expression, energy production, cytoskeletal dynamics, apoptosis and more. In neurons, Ca^{2+} ions also control neurotransmission (Berridge, 1998).

At rest, neurons maintain a low intracellular Ca^{2+} concentration ($[Ca^{2+}]_i$) in the 50–100 nM range (Helmchen et al., 1997; Maravall et al., 2000; Sabatini et al., 2002; Scott and Rusakov, 2006) compared to the high extracellular Ca^{2+} concentration ($[Ca^{2+}]_e$) of 1–3 mM (Jones and Keep, 1988; Egelman and Montague, 1999). Ca^{2+} is also concentrated in intracellular stores, such as in the lumen of the endoplasmic reticulum (ER), where its concentration is calculated to be ≈177 µM in resting neurons (Solovyova et al., 2002). To maintain these steep concentration gradients, neurons invest energy to control Ca^{2+} homeostasis. Low $[Ca^{2+}]_i$ is maintained through pumps, such as sarco/endoplasmic reticulum Ca^{2+}-ATPases (SERCAs) on the ER and plasma membrane Ca^{2+}-ATPases (PMCAs) on the plasma membrane (PM), and exchangers, for example Na^+/Ca^{2+} exchangers (NCXs) on PM and intercellular membranes (Brini et al., 2014).

In conjunction with these homeostatic mechanisms, the Ca^{2+} concentration gradient allows fast changes in $[Ca^{2+}]_i$ mainly through the activity of cytoplasmic Ca^{2+} channels, Ca^{2+} buffers and Ca^{2+} sensors (Brini et al., 2014). Voltage-gated Ca^{2+} channels (VGCCs or CaVs) and ligand-gated Ca^{2+} channels, such as α-amino-3-hydroxy-5-methyl-4-isoxazolepropionic acid (AMPA) and N-methyl-D-aspartate receptor (NMDA) receptors are situated on the PM and are responsible for cytoplasmic Ca^{2+} influx from the extracellular space (Clapham, 2007). Inositol triphosphate receptors (IP_3Rs) and ryanodine receptors (RyRs) are ligand-activated ion channels located at intracellular membranes. These channels regulate a flux of Ca^{2+} ions from the ER lumen into the cytosol and orchestrate a well-known pathway called Ca^{2+}-induced Ca^{2+} release (CICR). CICR is a specialized mechanism, by which an increase of $[Ca^{2+}]_i$ can evoke an amplification of Ca^{2+} release from the ER (Verkhratsky and Shmigol, 1996; Berridge, 1998).

Spontaneous neurotransmission

Action potential (AP)-independent neurotransmission is also called spontaneous release since it is independent of an AP and the triggering mechanism remains elusive. In contrast to evoked release or AP-dependent neurotransmission, spontaneous release often involves the release of a single synaptic vesicle (quantal release) which evokes a miniature excitatory postsynaptic current (mEPSC) (Fatt and Katz, 1950, 1952). Voltage-gated Na^+ (NaV) channels, which are highly important for the development and progression of the AP, are not required for spontaneous release, which still occurs in presence of the NaV blocker tetrodotoxin (TTX) (Narahashi, 2008).

Mechanism of spontaneous neurotransmission

The molecular mechanism of spontaneous release might be similar or different from evoked release and several hypotheses are currently under debate (Peled et al., 2014; Melom et al., 2013; Sara et al., 2005, 2011; Koenig and Ikeda, 1999; Atasoy et al., 2008; Kavalali, 2015; Fatt and Katz, 1952; Virmani et al., 2005; Verhage et al., 2000; Xu et al., 2009). To summarize briefly: spontaneous release might use different molecular machinery and/or molecular interaction; it might use a different pool of synaptic vesicles; it might occur in segregated sites within the synapses or in alternated synapses; it might have distinct postsynaptic targets; or the trigger might originate from distinct Ca^{2+} signalling pathways and involve distinct Ca^{2+} sensor proteins.

It is highly debated how spontaneous release is regulated by Ca^{2+}. Previous studies have reported that Ca^{2+} chelators like EGTA (ethylene glycol-bis(β-aminoethyl ether)-N,N,N',N'-tetraacetic acid) or BAPTA (1,2-bis(o-aminophenoxy) ethane-N,N,N′,N′-tetraacetic acid) reduce mEPSC events by ≈50% in hippocampal and pyramidal neurons (Ermolyuk et al., 2013; Simkus and Stricker, 2002). Increasing $[Ca^{2+}]_e$ leads to a higher mEPSC frequency; however, a complete removal of $[Ca^{2+}]_e$ does not fully abolish mEPSC (Xu et al., 2009; Groffen et al., 2010; Vyleta and Smith, 2011). On the one hand, some studies in neocortical neurons report that VGCCs are not involved in the mEPSC frequency increase by $[Ca^{2+}]_e$ (Vyleta and Smith, 2011). Other studies showed that the combined pharmacological blockade of several VGCC types decreases mEPSC frequency to 50% and in particular the R-type VGCC might play a role in spontaneous release in hippocampal synapses (Ermolyuk et al., 2013). This suggests that $[Ca^{2+}]_e$ and VGCC are partially involved in quantal neurotransmission but a substantial part of the spontaneous release is still maintained in their absence. Several studies support the idea that intracellular Ca^{2+} stores also contribute to trigger spontaneous neurotransmission, in particular, the CICR mechanism. The inhibition of either RyRs through ryanodine or IP_3Rs by 2-aminoethoxydiphenyl borate (2APB) decreases the mEPSC frequency in cortical pyramidal cells (Simkus and Stricker, 2002). Furthermore, caffeine induces an increase in mEPSC frequency (Simkus and Stricker, 2002; Xu et al., 2009). In summary, it is clear that Ca^{2+} has an important role in spontaneous release, but little is known about the exact source of the cytoplasmic Ca^{2+} signals and the molecular mechanisms that trigger quantal release events.

Ca^{2+} transients

Ca^{2+} rises can be spatially confined (local) or affect the whole cytoplasmic compartment of a cell (global). Local Ca^{2+} signalling could be induced by the opening of one or a cluster of channels (Augustine et al., 2003). AP-dependent Ca^{2+} influx is extensively documented. An AP generates a Ca^{2+} influx which is initially local, mainly localized at the presynapse and subsequently diffuses away to generate a more global Ca^{2+} rise. Koester and Sakmann (2000) combined two-photon microscopy and whole-cell recordings of the presynaptic pyramidal neurons of cortical layer 2/3 of juvenile rats loaded with Oregon Green BAPTA-1 (OGB-1), a

fluorescent Ca^{2+} indicator. They showed that the Ca^{2+} contribution to a single AP in the synaptic bouton is two-fold higher than in the axonal segment (Koester and Sakmann, 2000). During a single AP in the calyx of Held synapse, the $[Ca^{2+}]_i$ has been calculated to rise from 40 to 400 nM (Helmchen et al., 1997).

Several studies reported the existence of spontaneous Ca^{2+} events (SCEs) in living neurons. One study in 2000 by Llano et al. was performed in Purkinje cells treated with TTX. They observed, in parallel experiments, that the frequency of both mIPSCs and spontaneous Ca^{2+} transients (SCTs) increased after the application of ryanodine at a low agonistic concentration (5–10 μM) and in high extracellular Ca^{2+} (6 mM), reaching a SCT frequency of 0.019 Hz (Llano et al., 2000). SCTs were also recorded in hippocampal slice cultures, using OGB-1-AM, in presence of TTX, 1 μM nicotine and 10 mM Ca^{2+} in the extracellular solution (Emptage et al., 2001). This system detected a SCT frequency of 0.66 Hz, which was dramatically reduced by the antagonistic effect of 20 μM ryanodine. A more recent study detected SCTs in primary glutamatergic hippocampal neurons after TTX application. These SCTs showed a frequency 0.32 ± 0.04 min^{-1} per ROI which has been shown to depend upon extracellular Ca^{2+}, RyRs and NMDARs. The NMDAR-dependent events were postsynaptic (Reese and Kavalali, 2015).

In the present study, we define SCEs as all Ca^{2+} elevations that occur in absence of AP (i.e. in presence of TTX or by clamping neurons at -70mV), regardless of their kinetics. A commonly observed subclass, characterised by a local and short-lived Ca^{2+} increase (lifetime in the order of ms), is referred to as SCTs.

Visualising Ca^{2+} transients and synaptic vesicle release

Optical measurement of presynaptic Ca^{2+}-secretion coupling has been applied by co-expressing VGLUT1-mOrange2 or sypHTomato as red-shifted pH-sensitive vesicle exocytosis reporters with GCaMP, a genetically encoded Ca^{2+} indicator (GECI), in the same neuron stimulating release with APs (Li, 2011; Li and Tsien, 2012). Jackson and Burrone in 2016 fused the redshifted calcium indicator R-GECO1 (Zhao et al., 2011) and sypHy, a widely used pHluorin-derived vesicle exocytosis and endocytosis marker (Granseth et al., 2006), in a unique probe sypHy-RGECO and used it to observe the Ca^{2+} signals and secretory responses after stimulation with 1–20 APs (Jackson and Burrone, 2016).

Similar methods may also be applicable to study the suggested relation between Ca^{2+} dynamics and spontaneous release. For this purpose, we simultaneously measured SCEs and mEPSCs by imaging and electrophysiology in mouse neurons. Besides GCaMP6-based indicators, we utilize the fluorescent reporter JRex-GECO1 (Molina et al., 2019), a red-shifted Ca^{2+} indicator developed from REX-GECO1 (Wu et al., 2014) by the group of Prof. Campbell. A fusion of sypHy and JRex, together named sypHyJRex, was expressed in autapses and networks of cultured hippocampal neurons, providing important new insight in the involvement of presynaptic Ca^{2+} in quantal neurotransmission.

Materials and Methods

Primary neuron culture

Animals were housed, bred and experimentally used according to Institutional guidelines and Dutch and U.S. governmental laws with prior approval from the institutional animal research ethics committee ("Dierexperimentencommissie Vrije Universiteit/VU medisch centrum"; approval number FGA11-03), ensuring minimum discomfort of animals. Hippocampal and cortical neurons were obtained from C57BL/6 mouse brain tissue at embryonic day 18 (E18). After removal of the meninges, the hippocampi and the cortex were dissected in Hank's balanced salt solution (HBSS; Sigma, St. Louis, MO), which was buffered with 10 mM HEPES (Invitrogen, Carlsbad, CA). Cells were dissociated with 0.25% trypsin (Invitrogen) for 20 min at 37°C. After washing 5 times in HBSS, the cells were suspended and plated in Neurobasal medium (Invitrogen), supplemented with 2% B-27 (Invitrogen), 1.8% HEPES, 0.25% glutamax (Invitrogen) and 0.1% Pen-Strep (Invitrogen). Cells were triturated by three passes through fire-polished Pasteur pipettes and counted using a Fuchs-Rosenthal chamber.

Two types of culture were produced: high-density continental or micro-island cultures (Mennerick et al., 1995). For continental cultures, glass coverslips were pretreated by washing in 96% EtOH and then sprayed with a coating solution consisting of 0.1 mg/ml Poly-D-lysine (Sigma), 0.2 mg/ml rat tail collagen (BD Biosciences, Franklin Lakes, NJ) and 10.2 mM acetic acid (Sigma). For micro-island cultures, coverslips were etched with 1 N HCl for 2h, then washed, placed in 1 N NaOH for 1 h, and washed again. They were initially coated with 0.15% agarose, dried, and then stamped using a custom-built stamp (VU, The Netherlands) with a solution of 0.1 mg/ml Poly-D-lysine, 0.732 mg/ml rat tail collagen (BD Biosciences) and 10.2 mM acetic acid. Coverslips were sterilized under UV light for 20 min before plating glia. Continental high-density neuronal cultures were created by seeding 25k neurons/well over a layer of 25k rat glia cells/well on 18 mm coverslips in 12-well plates or 50k neurons/well on 50k rat glia cells/well for 25 mm coverslips in 6-well plates. Micro-island low-density neuronal cultures were prepared in 6 well plates by plating on 25 mm coverslip 3k neurons/well over micro-island 10k rat glia cells/well. Cultures were maintained in a humidified incubator at 37°C and 5% CO_2. Half of the medium was refreshed after 8 days.

Chemical Ca^{2+} indicators

For OGB-1 loading, cells were incubated with 1 µM OGB-1-AM (O6807; Molecular Probes, Eugene, OR) for 20 min at RT. For Fura-2 loading, 2.5 µM of Fura-2-AM (F1221; Thermo Fisher Scientific, Waltham, MA) was diluted in ACSF and applied for 15–20 min. In both cases, the coverslip was washed once in ACSF to remove a possible excess of the dye.

Plasmid and viruses

Neurons were infected with lentiviral infectious particles encoding synapsin-mCherry, GCaMP6s, GCaMP6f, syGCaMP6f, sypHy, syJRex or sypHy-

JRex between 0–9 DIV and used for experiments from 13 to 18 DIV. These constructs were cloned into a third-generation lentiviral expression vector derived from p156RRL and expressed by the neuron-specific synapsin or CaMKII promoters. Lentiviral infectious particles were prepared as described (Naldini et al., 1996). Synapsin-mCherry lentiviral expression was described previously (Geerts et al., 2017).

Lentiviral expression of GCaMP6 and synaptophysin-GCaMP6

SG524-AAV-hSyn1-GCaMP6s-P2A-nls-dTomato (AddGene #51084) and SG525-AAV-hSyn1-GCaMP6f-P2A-nls-dTomato (AddGene #51085) were kindly shared by Jonathan Ting. The 1437 bp BamHI – XbaI fragment was subcloned into the corresponding sites of SG527-pENTRrz1 (2677bp fragment) to yield SG529-pENTRrz1-GCaMP6f-P2A. To target GCaMP6f to synaptic vesicles, a fusion protein comprising zebrafish synaptophysin and GCaMP6f was generated. The 1378 bp BglII – KpnI fragment of SG542-Rib-SyGCamp6-10.500 was ligated into the 3571 bp BglII – KpnI vector fragment of SG529-pENTRrz1-GCaMP6f-P2A, resulting in plasmid SG543-pENTRrz1-SyGCaMP6f-P2A. To replace the P2A autocleavage signal with a stop codon after the C-terminus of GcaMP6f, the 203 bp PmlI-NotI fragment of SG529-GCaMP6f-P2A and SG543-pENTRrz1-SyGCaMP6f-P2A were replaced by the 128 bp PmlI-NotI fragment of SG542-Rib-SyGCamp6-10.500 (kindly provided by Leon Lagnado, University of Sussex, UK), yielding SG544-pENTRrz1-SyGCaMP6f-Stop and SG545-pENTRrz1-GCaMP6f-Stop. For lentiviral expression, Gateway LR cloning (Thermo Fisher Scientific) was used to generate pDEST-lenti-CaMKII(pr) expression vectors SG566-pDEST-LentiCaMKII-GCaMP6f and SG567-pDESTLenti-CaMKII-SyGCaMP6f. For GCaMP6s the same procedures were applied as for GCaMP6f.

Lentiviral expression of synaptophysin-pHluorin

For lentiviral expression of synaptophysin-pHluorin (sypHy), the P2A self-cleavage signal in SG546-pENTRrz1-mSyph(aa1–187)-pHluorin-mSyph(aa190–314)-P2A was replaced by a stop codon using a linker with cohesive ends ligated into the BamHI and XbaI sites. The linker was prepared by annealing oligonucleotides sg561 (5’-gatcagggatcctgagggcgatcgt-3’) and sg562 (5’-ctagacgatcgccctcaggatccct-3’). The resulting coding sequence of SG554-pENTRrz1-mSyph(1–187)-pHluorin-mSyph(190–314)-Stop was inserted into pDEST-syn(pr)LL3.7 by a LR reaction from the Gateway cloning system (Thermo Fisher Scientific). This vector uses a synapsin promoter for neuron-specific expression.

Lentiviral expression of synaptophysin-JRex

The oligonucleotides sg561 (5’-gatcagggatcctgagggcgatcgt-3’) and sg562 (5’-ctagacgatcgccctcaggatccct-3’) were annealed and ligated into the BamHI and XbaI sites of SG543-pENTRrz1-SyGCaMP6f-P2A, yielding SG563-pENTRrz1-mSyph-Stop. jRex-GECO1 was described previously. The 1290 bp BamHI – NotI fragment of SG550-pCDNA-JREX-GECO was ligated into the corresponding sites of SG563-pENTRrz1-mSyph-Stop. As a result, SG564-pENTRrz1-Sy-JREX

encodes a fusion protein composed of zebrafish synaptophysin and JRex, the latter located in the cytoplasmic compartment. The coding sequence was recombined into destination vector SG553-pDEST-syn(pr)LL3.7 by a LR reaction from the Gateway cloning system (Thermo Fisher Scientific).

Lentiviral expression of sypHyJRex

To express a single reporter molecule named sypHyJRex, which combines pHluorin in the SV lumen and JRex on the cytoplasmic face of synaptic vesicles, synaptophysin was used as a well-established marker. First, a synthetic linker sg561/sg562 was ligated into the BamHI and XbaI sites of SG546-pENTRrz1-mSyph(aa1–187)-pHluorin-mSyph(aa190–314)-P2A, resulting in SG554-pENTRrz1-mSyph(1–187)-pHluorin-mSyph(190–314)-Stop. The 1290 bp BamHI – NotI fragment of SG550-pCDNA-JREX-GECO was then inserted into the corresponding sites, yielding SG556-pENTRrz1-SyPhy-JREX. The coding sequence was recombined into the destination vector SG553-pDEST-syn(pr)LL3.7 by a LR reaction from the Gateway cloning system (Thermo Fisher Scientific). The resulting lentiviral expression vector was called SG600-pDESTsyn(pr)LL3.7-SyPhy-JREX.

Live imaging

Live cell imaging

Live cell imaging was performed using a custom-built epifluorescence setup called FAINT (for Flash activation of Action potential-Independent NeuroTransmission). It uses an inverted microscope (IX73; Olympus, Shinjuku, Tokyo) illuminated by a polychrome V monochromator (FEI, Munich, GmbH) with a 150 W Xenon high stability lamp in combination with a suitable green and red filter set (GFP # 49002 and mCherry # 49008; Chroma, Bellows Falls, VT). When specified, we used the Photometrics Dual-View 2 (Photometrics, Tucson, AZ) which was equipped with a T565lpxr dichroic mirror, and ET525/50 & ET605/70 emission filters (Chromaphor, Oberhausen, Germany). Images were acquired using a 40x (Olympus UAPON40xO340-2, NA 1.35) or 100x (Olympus UPLFLN100xO2/1.3U Plan Semi, NA 1.3) oil immersion objective and an Andor Ixon Ultra 897 electron-multiplying CCD (EM-CCD; Belfast, UK) camera, which was controlled by Live Acquisition software (v2.5.0.17; FEI) with the following settings: vacuum cooling to -70°C, EM gain of 200, pre-amplification of 2, 40% lamp intensity.

Coverslips were placed in the imaging chamber with ACSF as extracellular solution to enable simultaneous patch-recording containing (in mM): 140 NaCl, 2.4 KCl, 10 HEPES, 10 glucose, 4 $CaCl_2$, 4 $MgCl_2$ (pH 7.3, 300 mOsm); except otherwise specified. All chemicals were from Sigma Aldrich. 1 µM of tetrodotoxin (TTX; Ascent Pharmaceuticals, Islip, NY) was added when specified. To investigate the effect of different extracellular Ca^{2+} concentrations on SCEs and mEPSC, cells were patched in 2 mM Ca^{2+} extracellular solution, electrophysiology and imaging recordings were simultaneously started by Clampex 10.6 (Molecular Devices) using a TTL trigger and cells were perfused subsequently with ACSF containing 2, 0, 5 and 10 mM Ca^{2+} for 3 min each. Electrophysiology recordings were trig-

gered in the 3rd minute for each $[Ca^{2+}]_e$ step. This experiment was performed in presence of 1 µM TTX and 20 µM gabazine (Sigma Aldrich).

OGB-1 was excited at 485 nm. Genetically encoded probes GCaMP6, sypHy and syJRex, sypHyJRex were excited at a wavelength of 480 nm. Synapsis-mCherry was excited at a wavelength of 575 nm. Images were acquired for 1–12 minutes at a frequency of either 45 or 32 Hz for OGB-1, 0.1 Hz for Fura-2 (exposure duration of 500 ms with an interval of 6 seconds); 29 Hz or 18 Hz for GCaMP6, 29 Hz for sypHy and syJRex; either 3 Hz or 5 Hz for sypHyJRex.

Data were exported for further analyses in '.raw' or '.tif' format using the 'Offline Analysis' data streaming option in Live Acquisition software (FEI), together with its associated '.mtd' file, which contains metadata of the experiment. All images had a field dimension of 512 x 512 pixels with each pixel calibrated to cover 0.16 μm^2 (0.4 x 0.4 µm) for the 40x objective.

SypHyJRex imaging and controls

For dual channel simultaneous imaging of sypHyJRex, syJRex and either sypHy or syGCaMP6f, the Photometrics Dual-View 2 was used and the emission channels divided: channel 1 (red bandwidth of 570–640 nm corresponding to JRex emission) and channel 2 (green bandwidth of 500–550 nm corresponding to sypHy or syGCaMP6f emission).

SypHyJRex was imaged by a 100x objective with 2 x 2 camera binning (each pixel: 0.38 x 0.38 µm, field dimensions: 128 x 256 pixels) using Tyrode's solution (119 mM NaCl, 2.5 mM KCl, 4 mM $CaCl_2$, 1 mM $MgCl_2$, 30 mM glucose, 25 mM HEPES, pH 7.5); depolarizing solution (same as Tyrode's except for 61.5 mM NaCl, 60 mM KCl); NH_4Cl solution (same as Tyrode's except for 69 mM NaCl, 0 mM KCl, 50 mM NH_4Cl); acid-wash solution (as for Tyrodes's except for pH 5.5).

For comparisons of sypHy vs syJRex and of syGCaMP6f vs syJRex, neurons were imaged with a 40x objective with 2 x 2 camera binning (each pixel: 0.8 x 0.8 µm, field dimensions: 128 x 256 pixels) in ACSF. Perfusion media were identical to ACSF except for the listed components for sypHy vs syJRex: depolarizing solution (82.4 mM NaCl, 60 mM KCl), NH_4Cl solution (90 mM NaCl, 50 mM NH_4Cl), acid-wash solution (10 mM MES instead of HEPES; pH 5.5).

Image analysis

Image analysis of time lapse recordings was performed in three series of experiments with minor variations, detailed below.

Detection of Ca^{2+} transients reported by OGB-1-AM fluorescence

Images were bleach corrected using the built-in function of ImageJ (NIH). To highlight regions with spontaneous Ca^{2+} fluctuations, a $[F_t\text{-}F_{min}]_{max}$ image was calculated from the stack. ROIs were manually drawn on the entire neuronal structure. The mean fluorescence intensity of OGB-1-AM was measured for each frame in the time lapse using ImageJ. In Microsoft Excel, the mean intensity

value was corrected for the mean background intensity by subtraction, graphed and visually inspected for sudden changes in intensity. We searched for isolated Ca^{2+} events in the order of ms (SCTs). The $\Delta F/F_0$ was calculated in MATLAB (MathWorks 2015), using a F_0 value calculated as the average of the first 30 values in the time lapse. The $\Delta F/F_0$ values of SCTs were averaged for each cell and subsequently used to determine the amplitude and FWHM. The amplitude was calculated as maximum value of the $\Delta F/F_0$ trace minus the average of 10 data points 40 frames before the peak value. The FWHM was calculated as the time interval between the half-maximal signal during the rise and decay phase using the closest time points without sub-frame interpolation. SCT frequency for each cell was calculated as total number of events per cell, divided by the total acquisition time. Parameters per single cell were averaged to calculate the final average and SEM. The same procedure was used to detect evoked Ca^{2+} events (ECEs) triggered by electrophysiological stimulation except that in this case, four ROIs were used to average the evoked Ca^{2+} response per cell.

Detection of Ca^{2+} transients in GCaMP6-expressing neurons

After time lapse recording of GCaMP6s and GCaMP6f expressing neurons, the first 500 frames (17 s) were removed and the remaining frames were corrected for bleaching with the built-in function of ImageJ. To highlight regions with neuronal activity, an image was calculated to represent the standard deviation of all frames in the time dimension. The $\Delta F/F_0$ was calculated using a F_0 value calculated as the 25 last data points of the entire trace. All other procedures were as specified for OGB-1 AM fluorescence analysis. In the manual image analysis of GCaMP6f labelled cells in presence or absence of TTX, the ROIs were drawn randomly both in the pre- and in the post-TTX and the same ROIs were used to calculate mean intensity value in the paired recording data after correcting for possible translation or rotation using Align3_TP plug in of ImageJ (Parker, 2010). To assess if SCTs occurred in synapses or extrasynaptically, ROIs in which SCTs occurred were compared to a thresholded image mask reporting synapsin-mCherry fluorescence. The percentage of ROIs that co-localized with synapses was first calculated per cell. We then averaged those percentages to calculate the mean and SEM for all cells.

Ca^{2+} events assisted image processing

Image analysis of GCaMP6f labelled cells in presence or not of TTX, during perfusion of different Ca^{2+} concentrations and for the difference in SCEs detection between global GCaMP6f vs syGCaMP6f were performed with a custom written program called ‘supervised inspection of fast Ca^{2+} transients‘ (SICT) (Mancini et al., 2018, Chapter 2). Parameters were calculated for each individual Ca^{2+} event and then averaged per cell. Finally, the values were averaged to calculate the mean and SEM for all cells. The image analysis of GCaMP6f labelled cells in presence or not of TTX was also performed manually as earlier described.

Fura-2 ratiometric Ca^{2+} imaging analysis

The Fura-2-AM loaded neurons were recorded and perfused sequentially with

$[Ca^{2+}]_e$ of 0, 2, 5 and 10 mM. For ratiometric imaging of Fura-2, images were recorded at alternating excitation wavelengths of 340/380 nm in two separate channels. A mask was created on the max projection of the time lapse with a homemade MATLAB routine. The mask was then converted into a ROI in image J and the $F_{340/380}$ ratio calculated over time. The mean of the last 5 values at the end of each $[Ca^{2+}]_e$ perfusion was used to plot the relative $[Ca^{2+}]_i$ change against $[Ca^{2+}]_e$.

SypHyJRex image processing and controls

Time lapse sypHyJRex images were analysed using the Offline Analysis module version (v2.5.0.17) of Live Acquisition software (FEI). Mean intensity values were plotted from ROIs placed on visually detectable events and F/F_0 was calculated in Microsoft Excel. The F_0 was calculated as the average of 15 frames preceding the fluorescence increase onset.

Bleedthrough analysis and Ca^{2+} indicator comparison

To validate the quality of signal separation of channel 1(JRex) and channel 2 (sypHy or syGCaMP6f), we tested if fluctuations in JRex fluorescence intensity affect channel 2 and, vice versa, if fluctuations in sypHy fluorescence affect channel 1. For this purpose, either syJRex, sypHy or syGCaMP6f was expressed as the only fluorescent reporter and the emission in both channels measured. ROIs placed on visually detectable events. Intensities were corrected by background subtraction. The baseline fluorescence was calculated in the raw data as the average of 20 frames starting at 30 frames before each treatment (either by electrophysiological stimulation or with depolarizing, NH_4Cl or acid-wash solutions listed above). The raw amplitude was determined by the change in fluorescence intensity from baseline to maximum or minimum peak value after treatment. The percentage of bleedthrough was quantitated as the percentage of (signal observed in the non-specific channel) / (signal observed in the specific channel). Events with high amplitudes were selected for accurate bleedthrough estimation.

To compare Ca^{2+}-binding and -unbinding kinetics between syJRex and syGCaMP6f, Ca^{2+} events were evoked by a single AP or by 40 Hz train of 100 APs. Alternatively, SCTs were detected using SICT. To compare the sensitivity of syJRex and syGCaMP6f co-expressed in the same cell, the fluorescence in each channel was analysed using identical ROIs (i.e. with the same coordinates in time and space). For each ROI, the amplitude, 10-90% rise time, FWHM, and 90-10% decay time was calculated for the train stimulation. For the single AP, we measured amplitude and rise time because the FWHM and decay time were not assessable by SICT. The fluorescence intensity values over time were expressed as $\Delta F/F_0$ and averaged.

Electrophysiology recordings and analysis

Self-innervating glutamatergic hippocampal neurons from micro-island cultures were chosen for electrophysiological recordings between DIV14–18. The intracellular patch-pipette solution contained (in mM): 125 K^+-gluconic acid, 10 NaCl,

4.6 $MgCl_2$, 4 K_2 -ATP, 15 creatine phosphate (Calbiochem) and 10 U/ml phosphocreatine kinase (Calbiochem) (pH 7.3, 300 mOsm). The extracellular solution was ACSF, detailed in the live imaging section. Neurons were kept in ACSF for a maximum of 1.5 h at RT, which ranged from 21°C to 23°C. Recordings were performed with a MultiClamp 700B amplifier (Molecular Devices, San Jose, California). Digidata 1550 (Molecular Devices) and Clampex 10.6 were used for signal acquisition. Pipette resistance ranged from 2.5 to 5 MΩ. After whole-cell mode, series resistance was always 70% compensated, and only cells with a series resistance of <12 MΩ and a holding current of <500 pA were accepted for analysis. mEPSCs were recorded at a resting membrane potential of -70 mV at a sampling frequency of 10 KHz or 250 KHz. EPSCs were evoked by depolarizing the cell from −70 to +30 mV for 0.5 ms and recorded at a sampling frequency of 10 KHz. mEPSCs recordings were analysed by MiniAnalysis software (Synaptosoft Inc.), unless otherwise specified. mEPSC parameters of each recording were averaged to a single value before the mean of multiple cells was determined.

Temporal correlation mEPSCs/EPSCs and Ca^{2+} imaging

To acquire simultaneous electrophysiological and imaging recordings with precise temporal control, a TTL trigger signal was sent from Clampex 10.6 to LA software. To account to variable delays in the start of data acquisition, image acquisition started with a delay of two seconds. The EPSC and the voltage of the EM-CCD camera triggering signal were recorded in separate channels, allowing precise identification of the start and end times for each frame in the time lapse (**Figure S4**).

The Ca^{2+} events were analysed with SICT. For ECEs, about five different ROIs per cell were selected for each stimulation. We calculated the middle time between the start and end of frame acquisition for the frame where the $\Delta F/F_0$ peak signal occurred. The peak time of EPSCs and mEPSCs was determined from the electrophysiology recordings by a custom MATLAB program. The peak times from Ca^{2+} imaging and electrophysiology (SCTs/SCEs and mEPSCs, ECEs and EPSCs) were compared and mEPSCs that occur ± 1 s relative to a SCT were plotted in a histogram to allow the detection of temporally coupled events. In addition, the kinetic parameters of mEPSCs occurring within ± 250 ms relative to a SCT or a SCE were compared to mEPSCs outside that range. These kinetic parameters included amplitude, rise time and decay time, all calculated using custom-written code in MATLAB (Mathworks).

Immunocytochemistry and antibodies

Cells were infected at DIV9 with lentiviral particles encoding either GCaMP6f or syGCaMP6f driven by the neuron-specific CaMKII promoter. Cells were fixed at DIV15 with 3.7% formaldehyde for 30 min (Electron Microscopy Sciences, Hatfield, PA) and permeated with 0.5% Triton X-100 (Sigma) in phosphate-buffered saline (PBS) for 5 min at RT. Nonspecific antibody binding was prevented by incubation with blocking solution containing 2% normal goat serum and 0.1% Triton X-100 in PBS (pH 7.5) for 20 min at RT. Primary antibody anti-Synaptobre-

vin 2 (VAMPII; 104 211C3, SYSY, Göttingen, Germany 1:1000) and anti-MAP2 (ab5392, abcam, 1:500) incubation was done for 1h at RT. After washing with PBS 3 times, cells were incubated for 1h at RT with Alexa dye conjugated secondary antibodies (A21449, A11003, Life Technologies, Carlsbad, CA; 1:1000). Antibodies were diluted in blocking solution. After washing again, cells were mounted using Dabco-Mowiol (Calbiochem, San Diego, CA). Z-stack images were taken with a laser confocal Nikon Ti-E Eclipse microscope (Minato, Tokyo). Images were acquired using a 40x-oil immersion objective (NA 1.3) and areas with minimal glial background staining were selected.

Co-localization analysis

The co-localization analysis was performed using the coloc2-plugin of Fiji (https://imagej.net/Coloc_2). A neuronal mask was created based on a MAP2 fluorescence threshold using Fiji. The Pearson's R value (Manders et al., 1992) was assessed for 12 fields of view of neurons cultured from a single animal.

Statistical analysis

All statistical analysis was performed using SPSS v22.0 and v23.00 (IBM Corp., Armonk, NY, USA). All the data are reported as mean ± SEM, except when specified otherwise. Data were checked for normality using the Shapiro-Wilk or Kolmogorov-Smirnov test. When required, other assumptions were tested: the homogeneity of the variance was assessed with Levene's test and the sphericity assumption was tested with Mauchly's test. For normal distributed data, a parametric test was run; otherwise, a non-parametric test was performed. Moreover, if the sphericity assumption was not met the Greenhouse-Geisser correction was used to adjust the degree of freedom. For two groups, paired samples t-test or Wilcoxon signed-rank test and independent samples t-test or Mann-Whitney U test were performed. In the case of more than 2 groups, one-way repeated measure ANOVA or Friedman test was used. For each experiment, the p-value alpha significance threshold was adjusted for the number of multiple tests performed. In the case of multiple groups, Bonferroni correction was used to adjust the p-value for pairwise comparison keeping the p-value alpha significance threshold at 0.05. The effect size was calculated for the paired samples t-test as $r = \sqrt{(t^2 / (t^2+df))}$, for Wilcoxon signed-rank test as $r = |Z / (\sqrt{N})|$, for one-way repeated measures ANOVA as $r = \sqrt{(\eta^2)}$ and for Friedman test as $r = \sqrt{(\chi^2 / (N+\chi^2))}$. The effect size is reported for all p-values lower than 0.05. In the box plots of each figure, the empty dots represent the single parameter value. The filled dot depicts the mean of the empty dots ± SEM. The central line shows the median and red 'plus' symbols mark the statistical outliers which were included in the analysis. The statistical analysis summary for each experiment is reported in the **Supplementary Table 1** which also contains the sampling number (n) and the number of independent experiments (N) which represents an individual nest.

Results

Detection of fast spontaneous Ca^{2+} transients in hippocampal neurons

To detect spontaneous Ca^{2+} transients, hippocampal neurons in autaptic culture were loaded with OGB-1-AM (**Figure 1A**). Simultaneous imaging and whole cell voltage clamp recording was performed at a resting membrane potential of -70 mV. $\Delta F/F_0$ signals over time were plotted for many ROIs, together covering the full neuronal morphology (**Figure 1B**). Isolated SCEs (i.e. spontaneous Ca^{2+} events) occurred at different times in different neurites distributed over the microscopic field. Many SCEs showed similar dynamics, featuring a fast $\Delta F/F_0$ increase followed immediately by a quick decay to baseline, thus causing a transient peak FWHM of less than 0.2 s (**Figure 1C-F**). We called this class of events SCTs (for transients). They were observed in 7 of 8 cells with a mean frequency of 0.6 ± 0.19 Hz. For a quantitative description, the $\Delta F/F_0$ of these SCTs were averaged per cell and their frequency, amplitude and kinetic parameters were calculated

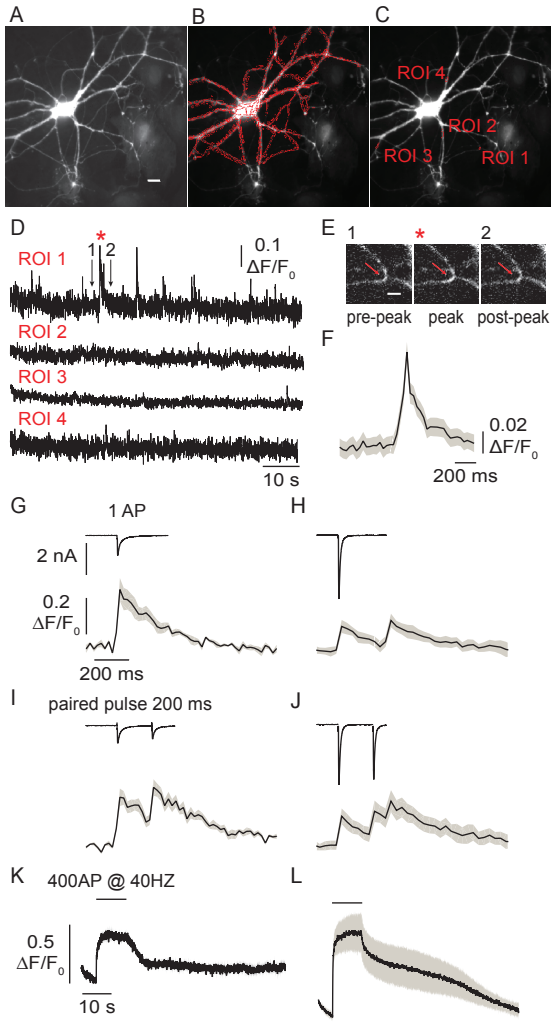

Figure 1. Detection of spontaneous Ca^{2+} transients and evoked Ca^{2+} events with OGB-1. (**A**) Typical example image of neurons described in **Table 1**, labelled for 20 min with 1 µM OGB-1-AM. Hippocampal neurons were plated on glial microislands. Whole cell voltage clamp recording and time lapse imaging were performed simultaneously. Scale bar 10 µm. (**B**) Regions of interest (ROIs) were manually drawn on the whole neuronal structure. (**C**) ROIs for which the fluorescence intensity is depicted in **D**. (**D**) Example of OGB-1 $\Delta F/F_0$ traces acquired at a resting membrane potential of -70 mV for ROIs highlighted in C. (**E**) OGB-1 fluorescence in image frames taken shortly before (1), during (*) and after (2) the peak highlighted in **D** (ROI1). Scale bar 5 µm. (**F**) Average $\Delta F/F_0$ profile ± SEM for all 61 SCTs detected in the represented cell (cell 2, **Table1**). (**G**-**L**) Average $\Delta F/F_0$ values ± SEM from 4 ROIs of a single cell corresponding to cell 6 (**G**, **I**, **K**) and cell 2 (**H**, **J**, **L**) after presynaptic depolarization. (**G**-**H**) Two representative examples of Ca^{2+} kinetics evoked by a single AP; upper panel shows EPSC and lower panel shows OGB-1 $\Delta F/F_0$ response. The Ca^{2+} signal depicted in **H** showing two Ca^{2+} peaks is detailed in **Supplementary figure 1**. (**I**-**J**) EPSC (upper panel) and $\Delta F/F_0$ (lower panel) response elicited by two APs at a 200 ms interval. (**K**-**L**) Average $\Delta F/F_0$ signal evoked by a 40 Hz train stimulation of 400 APs. Black bar indicates the stimulation period. Unit scaling in **G** is identical to **H**, **I** and **J**. Scaling in **K** is identical to **L**.

(**Table 1**). The SCTs detected with OGB-1-AM had an average frequency of 0.6 Hz and FWHM of 49 ms. To evoke Ca^{2+} transients, the same neurons were stimulated with a single AP, with two APs given with an interval of 200ms, and with a train of 400 APs at 40 Hz (**Figure 1G-L**). In contrast to the SCEs, the evoked Ca^{2+} events (ECEs) were evident in all ROIs over the entire neuron. ECEs occurred in all 8 cells. The amplitude and the peak duration were calculated averaging four ROIs per cell (**Table 1**). On average, the amplitude of the OGB-1 signal was approximately four times larger for ECEs triggered by a single AP than for

Table 1. Evoked Ca^{2+} event and spontaneous Ca^{2+} transient parameters detected with OGB-1. Eight neurons dissociated from the mouse hippocampus (n = 3, white rows) or cortex (n = 5, grey rows) were cultured on glial microislands. Spontaneous and evoked Ca^{2+} events were measured by OGB-1-AM fluorescence imaging as $\Delta F/F_0$ traces. For SCTs, the total number of detected events, their frequency, amplitude, FWHM and decay tau are indicated for each cell. For ECEs, the signal amplitude and FWHM are indicated for each cell in response to a single AP, a paired pulse of 200 ms and a 40 Hz train of 400 APs. Asterisks (*) indicate cells that showed two Ca^{2+} peaks in response to single AP as specified in **Figure 1H.**

	Spontaneous Ca^{2+} transients (STCs)					**Evoked Ca^{2+} events (ECEs)**					
						single AP		200 ms paired pulse		400 AP @ 40 Hz	
cell (ID)	number per cell	frequency (Hz)	amplitude ($\Delta F/F_0$)	FWHM (s)	decay Tau (s)	amplitude ($\Delta F/F_0$)	FWHM (s)	amplitude ($\Delta F/F_0$)	FWHM (s)	amplitude ($\Delta F/F_0$)	FWHM (s)
1	61	0,54	0,045	0,095	0,12	0,047	0,158	0,051	0,156	0,097	9,95
2*	61	0,78	0,085	0,095	0,15	0,156	0,189	0,238	0,284	0,732	30,78
3	12	0,11	0,160	0,032	0,03	0,113	0,063	0,218	0,221	0,348	13,02
4*	-	-	-	-	-	0,224	0,408	0,244	0,537	0,151	10,80
5	5	0,06	0,123	0,022	0,01	0,583	0,129	0,969	0,301	1,395	12,13
6	109	1,40	0,090	0,043	0,13	0,305	0,172	0,31	0,301	0,362	12,09
7	80	1,03	0,052	0,043	0,09	0,502	0,129	0,639	0,215	1,065	12,82
8	42	0,37	0,066	0,016	0,04	0,421	0,158	0,516	0,252	0,971	14,92
average	52,86 ± 12,99	0,613 ± 0,173	0,089 ± 0,015	0,049 ± 0,012	0,081 ± 0,019	0,294 ± 0,068	0,176 ± 0,036	0,398 ± 0,104	0,283 ± 0,040	0,640 ± 0,167	14,56 ± 2,38

SCTs (a full list of the parameter ratio is shown in **Table 2**). In most cells a single AP caused a single peak in OGB-1 fluorescence (see **Figure 1G**). In two cells however, a single AP caused two Ca^{2+} peaks. In those cases, the second Ca^{2+} peak was not associated with a second postsynaptic EPSC (**Figure 1H** and **Supplementary Figure 1**). Repeated stimulation caused an additive $\Delta F/F_0$ increase that could be separated after 200 ms paired pulse stimulation (**Figure 1I-J**), but not during a 40 Hz stimulation train (**Figure 1K-L**). We next compared the performance of GCaMP6s and GCaMP6f. As reported previously (Chen et al., 2013) after single and multiple AP stimulations, the $\Delta F/F_0$ amplitude of GCaMP6s amplitude is 2-fold larger than that of GCaMP6f. In our experiments, both GCaMP6s and GCaMP6f expressing neurons (**Figure 2A-D**) showed Ca^{2+} transients in non-stimulated cells (**Figure 2E-F**) with the same signal intensity (**Figure 2G-K**). From the three Ca^{2+} indicators tested, GCaMP6f produced the best signal-to-noise ratio (SNR of 57 with a FWHM of 282 ms), compared to GCaMP6s (SNR of 46 and FWHM of 412 ms) and OGB-1-AM (FWHM of 49 ms and SNR of 23). In view of the importance of detection sensitivity (i.e. SNR) and other advantages of GECIs, and despite the faster kinetics of OGB-1, we selected GCaMP6f for further experiments.

Table 2. Ratio between evoked Ca^{2+} event and spontaneous Ca^{2+} transient parameters. Amplitude and FWHM ratio between ECEs and SCTs for each cell analysed in **Table 1**. Total of 7 cells, 3 from hippocampus (white rows) and 4 from cortex (light grey rows). Asterisk (*) indicates a cell that showed two Ca^{2+} peaks in response to single AP as specified in **Figure 1H**.

	AMPLITUDE RATIO (Evoked/Spontaneous)			FWHM RATIO (Evoked/Spontaneous)		
cell (ID)	AP	PP	TRAIN	AP	PP	TRAIN
1	1,044	1,133	2,156	1,663	1,642	104,78
2*	1,835	2,800	8,612	1,989	2,989	323,98
3	0,704	1,359	2,170	1,993	6,991	411,86
5	4,740	7,878	11,341	5,864	13,682	551,27
6	3,389	3,444	4,022	4,000	7,000	281,05
7	9,654	12,288	20,481	2,999	4,999	298,00
8	6,379	7,818	14,712	9,987	15,929	942,79
average	3,964 ± 1,223	5,246 ± 1,577	9,070 ± 2,620	4,071 ± 1,132	7,605 ± 2,015	416,25 ± 101,57

Ca^{2+} transients are independent of APs

The SCTs detected with OGB-1 are likely independent of APs because they were observed at a resting membrane potential of -70 mV. To further test this idea, we measured Ca^{2+} transients with GCaMP6f in the same cells in absence and presence of 1 µM TTX to block AP propagation (**Supplementary Figure 2A**) and analysed them manually (**Supplementary Figure 2**) or with SICT (Mancini et

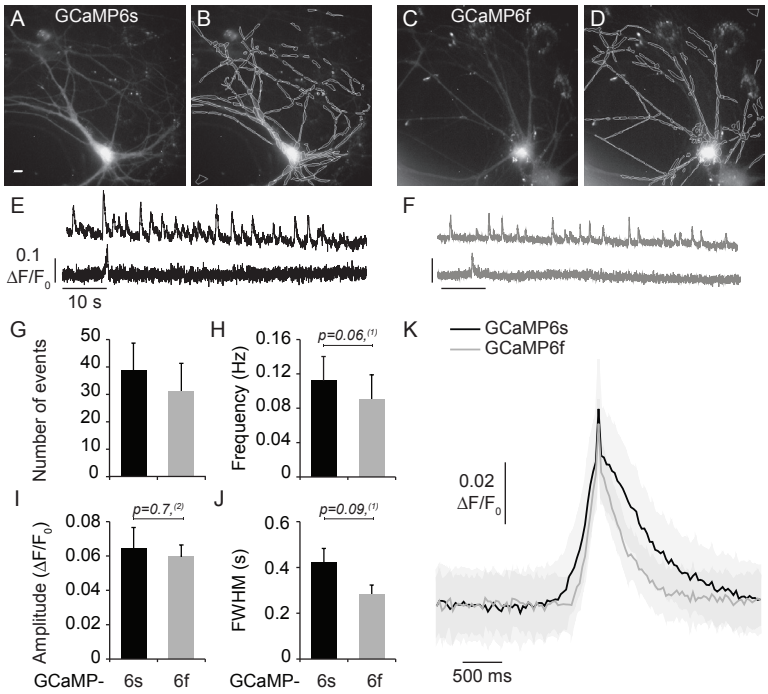

Figure 2. GCaMP6s vs GCaMP6f in Ca^{2+} transient detection. (**A**-**D**) Example images of GCaMP6s (**A**-**B**) and GCaMP6f (**C**-**D**) fluorescence, expressed using lentiviral vectors using the neuron-specific synapsin promoter. Scale bar 10 µm. Neurons were imaged in absence of external stimulation. (**B**, **D**) ROIs were manually drawn on the whole neuronal structure to detect Ca^{2+} transients as in **Figure 1**. (**E**, **F**) $\Delta F/F_0$ traces using GCaMP6s (black) and GCaMP6f (grey) in non-stimulated cells from two example ROIs. (**G**) Mean number of events during approximately 5 min of recording and (**H**) frequency of Ca^{2+} transients detected in cells expressing GCaMP6s (n = 9 cells) and GCaMP6f (n = 8 cells). (**I**) Amplitude. (**J**) FWHM. (**K**) Average $\Delta F/F_0$ profile of Ca^{2+} transients detected by GCaMP6s (black, n = 9) and GCaMP6f (grey, n = 8) Error bars indicate SEM. The statistical significance was assessed using (1) Independent samples t-test, (2) Mann-Whitney U test.

al., 2018), a semi-automated image processing tool to extract Ca^{2+} transient parameters (**Figure 3**). Signal intensity was measured as $\Delta F/F_0$ amplitude (**Figure 3A**) and, also, as integrated amplitude which takes into consideration the size of the ROIs (**Figure 3C**). The automated analysis showed no effect of TTX on the signal intensity (**Figure 3A,C**) whereas the manual analysis suggested a higher amplitude after TTX application (**Supplementary Figure 2D**).

The latter effect may be an artefact related to bleaching, causing a lower SNR (see **Supplementary Figure 2B**). Both analyses showed no effect on kinetic parameters (**Figure 3D-F** and **Supplementary Figure 2E**) and no alteration in the frequency of fast Ca^{2+} transients (**Figure 3H** and **Supplementary Figure 2G**), which presented similar kinetic properties as shown earlier (**Supplementary Figure 2C** and **Figure 2K**).

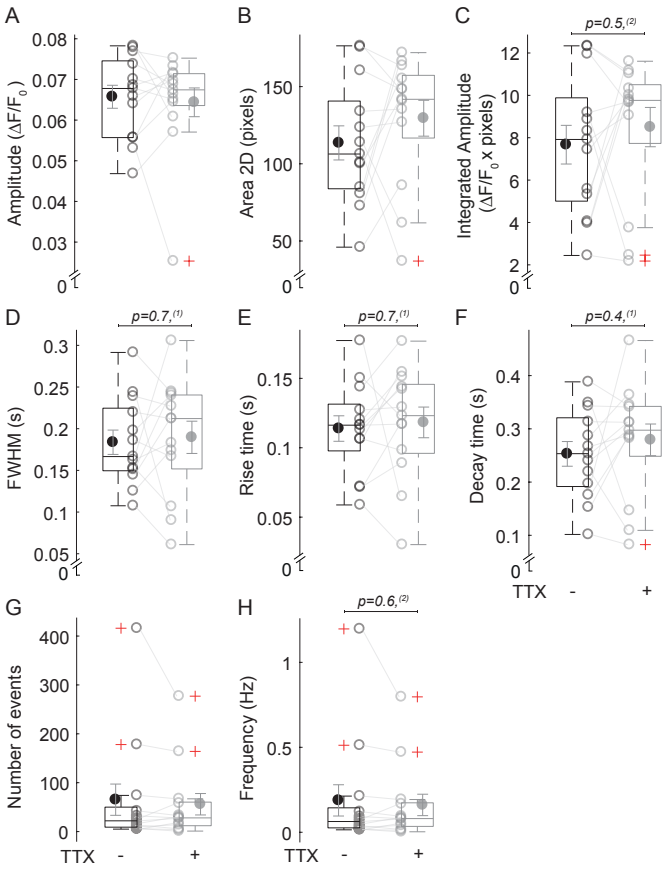

Figure 3. Effect of TTX on Ca^{2+} transients. Ca^{2+} transients were analysed prior to and after the addition of 1 µM TTX in hippocampal continental neurons expressing GCaMP6f using SICT for semi-automated image processing. (**A**) Amplitude of the $\Delta F/F_0$ signal during SCTs. (**B**) ROI Area 2D. (**C**) Integrated amplitude (amplitude x ROI area in pixels). (**D**) FWHM. (**E**) Rise time. (**F**) Decay time. (**G**) Number of events. (**H**) Frequency. The box plots show SCT parameters with empty dots representing the average value per cell and filled dot representing the mean ± SEM of all cells. The central line shows the median. Statistical outliers are marked by red 'plus' symbols. The statistical significance was tested using (1) Paired samples t-test, (2) Wilcoxon signed-rank test (n = 13 cells). A manual analysis of the same dataset is depicted in **Supplementary Figure 2**.

Besides the typical SCTs described above (**Supplementary Figure 3A**), other types of spontaneous Ca^{2+} events were also observed (**Supplementary Figure 3B**). These events were not characterised by a consistent signal pattern and are further referred to as 'complex' SCEs. Fast isolated Ca^{2+} transients (SCTs) are the most abundant class of events (59.7% of all SCEs). Instead, complex SCE present a minority (40.3% altogether) and include several types of kinetics: a combination of fast and slow Ca^{2+} rises (18.9%); multiple fast Ca^{2+} transients (9.6%); slow isolated Ca^{2+} transients ('SlowSingle'; 6.0%); and other rare event types, such as drift in baseline fluorescence and Ca^{2+} waves (Mancini et al., 2018). Given the heterogenic nature of complex SCEs, we do not provide descriptive parameters for these events.

Spontaneous Ca^{2+} transients are enriched in synapses

Next, we investigated if SCTs occur in synapses. By time lapse imaging in primary neurons expressing GCaMP6f and synapsin-mCherry, we found that 70% of the ROIs, which presented one of more SCTs, co-localize with synapsin (**Figure 4**). To directly measure presynaptic Ca^{2+}, we fused GCaMP6f to the C-terminus

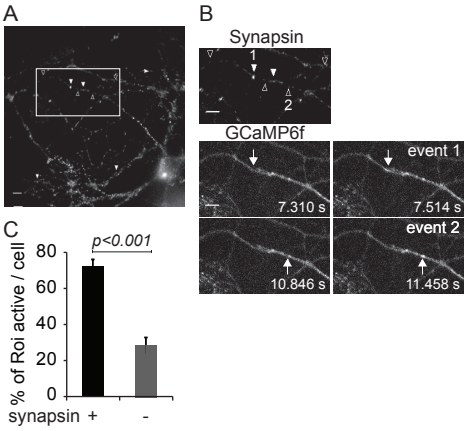

Figure 4. SCTs occur predominantly in synapses. (**A**) Representative fluorescence image of a neuron expressing synapsin-mCherry used to colocalize GCaMP6f-detected SCTs to synapses (filled arrowheads) or extrasynaptic structures (empty arrowheads). White rectangle indicates zoomed region in **B** (upper panel); scale bars 10 µm. (**B**) Zoomed image frames of a neuron showing synapsin-mCherry (top image) or GCaMP6f fluorescence (bottom panels), before (left panels) or during each of 2 SCT events (right panels); arrows depict the events. (**C**) Percentage of ROIs (each showing one or more SCTs) per cell that co-localize (black) or not (grey) with synapsin-mCherry. SCTs occur significantly more often in synapsin-positive structures (Mann-Whitney U Test, n = 43 cells).

of synaptophysin, a well-established marker of synaptic vesicles. In contrast to global GCaMP6f, synaptophysin-GCaMP6f (syGCaMP6f) co-localized well with VAMPII (synaptobrevin-2) immunoreactivity, confirming the specificity of synaptic targeting (**Figure 5**).

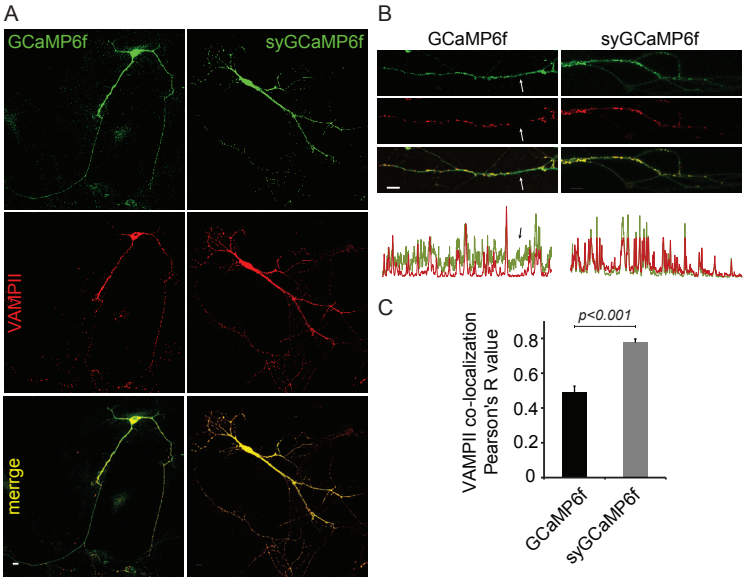

Figure 5. Synaptic targeting of GCaMP6f: syGCaMP6f. (**A**) Confocal images of hippocampal neurons expressing GCaMP6f (green) and stained for VAMPII (red). Upper panels show GCaMP6f without (left) or with (right) synaptophysin fusion (syGCaMP6f). Middle panels show VAMPII immunoreactivity. (**B**) Zoomed neuronal region with corresponding distribution intensities (bottom) of either GCaMP6f (upper left panel, green) or syGCaMP6f (upper right panel, green) with VAMPII (middle panel, red). Bottom panels in **A** and **B** show merged images (scale bar 10 µm). (**C**) Degree of synaptic localization was calculated as Pearson's R value to quantitate the co-localization of GCaMP6f with the synaptic vesicle marker VAMPII. syGCaMP6f yielded a significantly higher correlation compared to global GCaMP6f; independent samples t-test (n = 12 cells each for GCaMP6f and syGCaMP6f).

SyGCaMP6f detected SCTs with similar signal intensity as global GCaMP6f (**Figure 6B,D**) and similar kinetic properties (**Figure 6E**), except that the signal was restricted to a 1.24-fold smaller area (**Figure 6C**). Moreover, syGCaMP6f detected 2.5-fold more SCTs compared to global GCaMP6f (**Figure 6H-I**). The number of complex SCEs was unchanged (**Figure 6J**). We conclude that syGCaMP6f is a suitable reporter for presynaptic SCTs and that the number of events detected with this reporter is substantially higher than with general, soluble GCaMP6f.

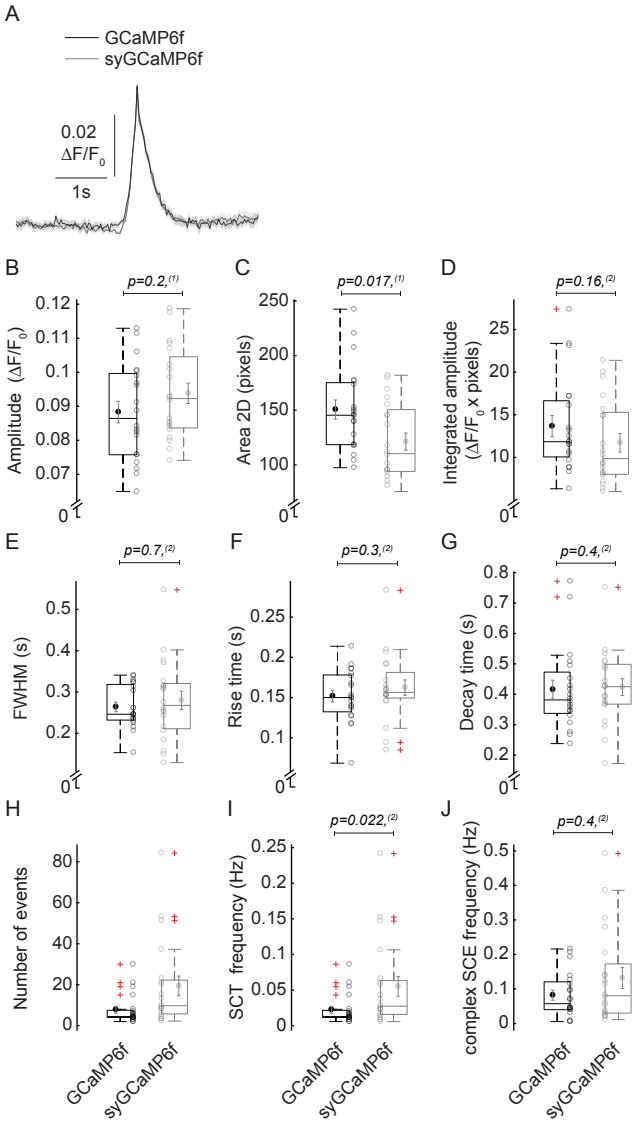

Figure 6. SCE detection using global GCaMP6f and syGCaMP6f. (**A**) Average $\Delta F/F_0$ trace ± SEM of all detected SCTs with GCaMP6f (black) or with syGCaMP6f (grey) analysed with SICT. Traces were first averaged to calculate the mean trace per cell, and then averaged to calculate the mean ± SEM from n = 20 cells. (**B**-**I**) SCT parameters detected with either GCaMP6f (black) or syGCaMP6f (grey). (**B**) Amplitude. (**C**) ROI Area 2D. (**D**) Integrated amplitude (amplitude x pixels). (**E**) FWHM. (**F**) Rise time. (**G**) Decay time. (**H**) Number of events. (**I**) Frequency of SCTs. (**J**) Frequency of complex SCEs. Empty dots represent average values per cell; filled dots depict the mean ± SEM of all cells. Central line shows median and statistical outliers are marked by red 'plus' symbols. The statistical significance was tested with (1) Paired samples t-test; (2) Wilcoxon signed-rank test (n = 20 cells for each GCaMP6f and syGCaMP6f).

Global and spontaneous Ca^{2+} events during $[Ca^{2+}]_e$ perfusion

Increased extracellular Ca^{2+} concentrations are known to elevate mEPSC frequencies in neurons. We studied if this phenomenon is related to global changes in $[Ca^{2+}]_i$ or the frequency and dynamics of SCEs (**Figure 7**). First, to measure the effect of $[Ca^{2+}]_e$ on global $[Ca^{2+}]_i$, we loaded autaptic hippocampal neurons with Fura-2-AM and measured the F_{340}/F_{380} nm ratio during perfusion with various $[Ca^{2+}]_e$ from 0 mM to 10 mM (**Figure 7A-C**). As expected, the mean F_{340}/F_{380} ratio increased significantly from 0,28 to 0,33, reaching a steady state within a minute after each buffer change (**Figure 7C**), indicating a significant increase in global $[Ca^{2+}]_i$. As control, neurons were perfused for the same duration in 0 mM $[Ca^{2+}]_e$ (**Figure 7B**, grey).

Second, we assessed the effect of $[Ca^{2+}]_e$ on mEPSCs and SCEs by simultaneously recording postsynaptic currents and syGCaMP6f fluorescence. In this case, to aid in establishing seals for electrophysiology, the order of the buffers was changed to 2, 0, 5 and 10 mM sequentially. For each $[Ca^{2+}]_e$ concentration, mEPSC parameters are shown in **Figure 7D-H**. There was a highly significant correlation between the mean mEPSC frequency and $[Ca^{2+}]_e$, increasing from 12 Hz at 0 mM to 22 Hz at 10 mM (**Figure 7E**). The mEPSC amplitude was reduced from 17 pA at 2 mM to 12 pA at 10 mM $[Ca^{2+}]_e$ (**Figure 7F**). The mEPSC rise time and decay time were not dependent on $[Ca^{2+}]_e$ (**Figure 7G,H**).

To investigate if the $[Ca^{2+}]_e$ elevation affected the frequency and characteristics of SCEs reported by syGCaMP6f imaging, we first quantitated the SCTs, while excluding the complex SCEs (**Figure 7I-P**). The SCT frequency (**Figure 7J**), amplitude (**Figure 7K,P**) and ROI size (**Figure 7L**) were not significantly affected by changes in $[Ca^{2+}]_e$ and concomitant changes in $[Ca^{2+}]_i$. Kinetic parameters were also not affected (**Figure 7M,O**), except for the SCT decay time which increased at higher $[Ca^{2+}]_e$ (**Figure 7N**). In a second analysis, we considered all SCEs (both SCTs and complex SCTs; **Figure 7Q-S**) and found a significant rise in SCE frequency from 0,4 ± 0,1 to 1,1 ± 0,2 Hz (**Figure 7Q**). The overall correlation between mEPSC and all SCE frequency remained poor (**Figure 7S**).

Taken together, this experiment indicates that $[Ca^{2+}]_e$ elevation increases global $[Ca^{2+}]_i$, and the frequency of complex SCEs, but not SCTs, and prolongs the decay of fast SCTs.

mEPSC are not tightly coupled to SCEs in the time dimension

Previous analyses showed a correlation in frequency between SCEs and mEPSCs in parallel experiments (Emptage et al., 2001; Llano et al., 2000; Reese and Kavalali, 2015; Ermolyuk et al., 2013). To measure SCEs and mEPSCs simultaneously in the same cells, autaptic neurons were simultaneously voltage clamped and time lapse imaged. To precisely control the timing of electrophysiology and image data, the camera shutter signal was also recorded (see method section and **Supplementary Figure 4**).

As a positive control, we calculated the temporal correlation between the EPSC

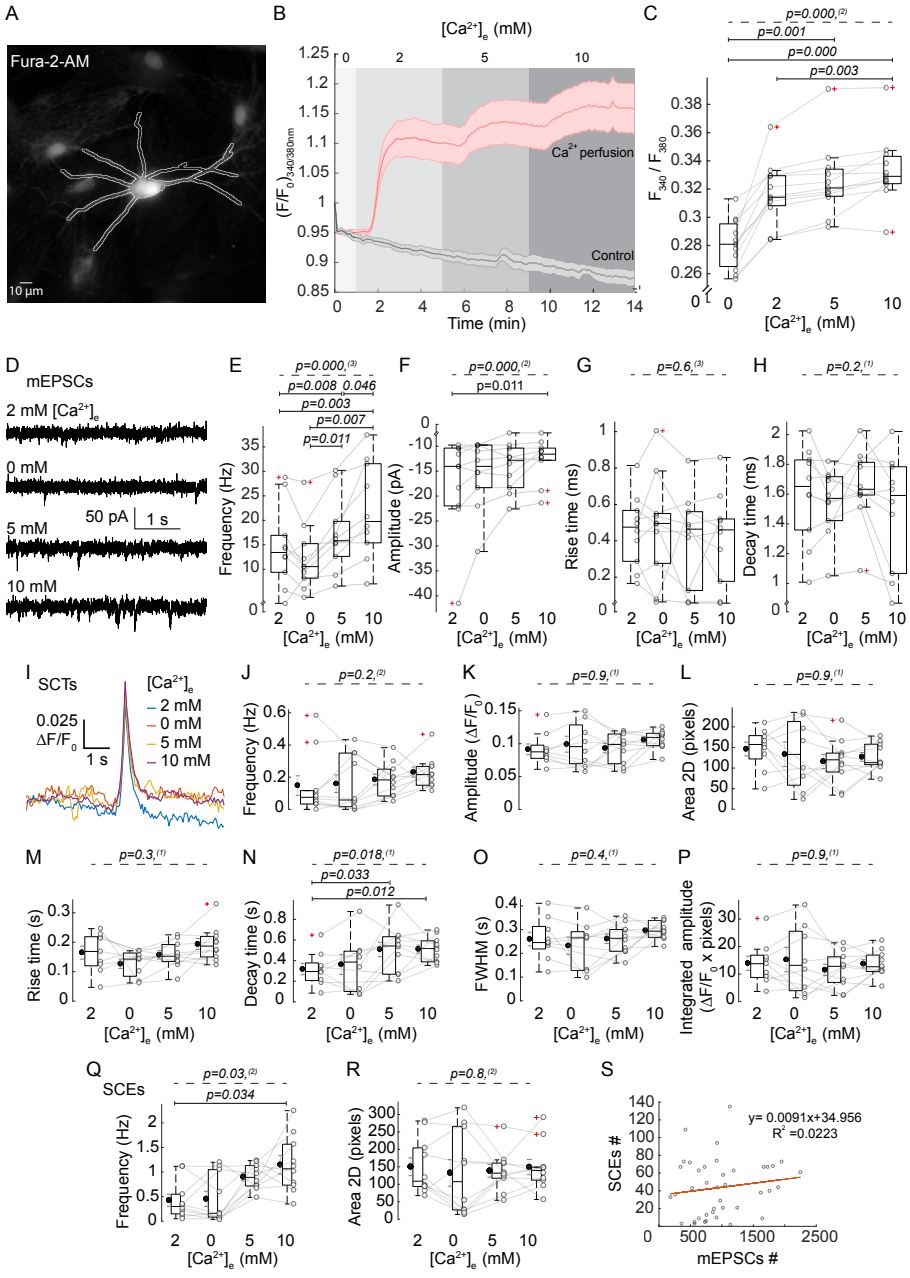

Figure 7. $[Ca^{2+}]_e$ affects global $[Ca^{2+}]_i$, SCT decay and SCE frequency. (**A**-**C**) Ratiometric Ca^{2+} imaging in Fura-2-AM loaded neurons during perfusion with varying $[Ca^{2+}]_e$. (**A**) Maximal projection in the time dimension of a representative time lapse recording. The white outline depicts the ROI used during the entire recording for $F_{340/380}$ nm ratiometric kinetic measurement. (**B**) Mean $F/F_{0\ (340/380nm)}$ trace ± SEM of global $[Ca^{2+}]_i$ during $[Ca^{2+}]_e$ perfusion from 0 to 10 mM (red) and for control neurons perfused with 0 mM for the same duration (grey). (continue on next page)

(continued from previous page) (**C**) Average $F_{340/380}$ nm ratio at the end (last 24 s) of each $[Ca^{2+}]$ perfusion. The $[Ca^{2+}]_e$ increase is accompanied by an increase in $[Ca^{2+}]_i$. Statistical significance was tested using Friedman test (n = 10 cells). (**D**-**S**) Simultaneous electrophysiology and Ca^{2+} imaging recording in syGCaMP6f expressing neurons. Neurons were first patched in presence of 2 mM $[Ca^{2+}]_e$ and subsequently perfused with 0, 5, 10 mM Ca^{2+}. (**D**) Typical example of mEPSCs during each perfusion step. (**E**-**H**) Quantitation of mEPSC parameters. (**E**) Frequency. (**F**) Amplitude. (**G**) Rise time. (**H**) Decay time. (**I**-**P**) Quantitation of SCT parameters (**I**) Average $\Delta F/F_0$ trace of SCTs occurring during each $[Ca^{2+}]_e$ perfusion. (**J**) Frequency. (**K**) Amplitude. (**L**) Area 2D. (**M**) Rise time. (**N**) Decay time. (**O**) FWHM. (**P**) Integrated amplitude. (**Q**-**S**) Quantitated parameters of all SCEs (**Q**) Frequency (**R**) Area 2D (**S**) Correlation plot showing the number of all types of SCEs vs mEPSCs observed per condition per cell (4 conditions x 10 cells). Statistical significance was assessed using [(1)] One-way repeated measures ANOVA, [(2)] Friedman Test, [(3)] One way repeated measures ANOVA with Greenhouse-Geiser correction (n = 11 cells).

and ECE triggered by a single AP (**Figure 8A**). The peak signal from the Ca^{2+} indicator syGCaMP6f occurred 50–150 ms after the EPSC peak signal. Despite this delay, a strict temporal correlation was evident when the plotting the relative timing of the EPSC and ECE peaks in a histogram (29 cells, **Figure 8B**).

The same procedure was used to investigate the relative timing of mEPSCs and SCEs. In a first analysis, we selectively investigated SCTs (**Figure 9**). A strict dependence of mEPSCs on SCTs was not observed. Some cells exhibited high mEPSC frequencies while the SCT frequencies were low, but some cells which had higher mEPSC frequencies also had higher SCT frequencies (**Figure 9A**). **Figure 9B** shows the average mEPSC from 29 cells. Moreover, the mEPSCs that occurred within ± 1 s relative to SCTs occurred with a similar probability before or after the SCE peak (**Figure 9C**, data from 29 cells). To investigate if the mEPSCs that might be coupled to SCTs could have different features, we compared the properties of mEPSCs that occurred within ± 250 ms relative to a SCTs with the properties of all other mEPSCs. The amplitude, rise time and decay times are plotted in **Figure 9D-F**. These mEPSCs had a slightly lower amplitude than the other mEPSC, 21 and 23 pA respectively (r = 0.07) but no difference in mEPSC rise and decay times (**Figure 9G-I**).

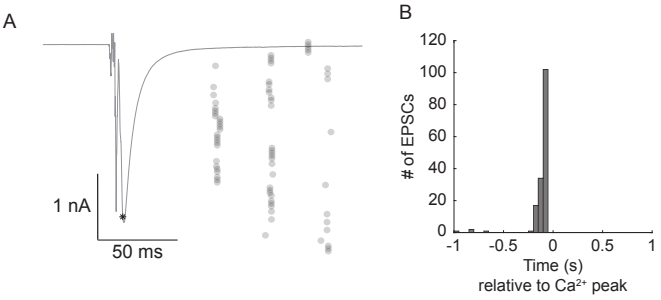

Figure 8. Detection of ECEs and EPSCs induced by a single AP in the same neurons expressing syGCaMP6f. (**A**) Averaged single EPSC from n = 29 autaptic neurons; the asterisk indicates the average time in which the maximum of the EPSC occurred. Grey circles indicate the time when the maximum of the evoked Ca^{2+} response was induced by single AP (their discrete time distribution reflects the imaging framerate). For each cell, a single EPSC is plotted together with multiple Ca^{2+} events (an average of 5 per cell). (**B**) Histogram showing the number of EPSCs detected within ± 1 s from the ECE peak. The Ca^{2+} response was detected with a delay of 150 ms after the EPSC.

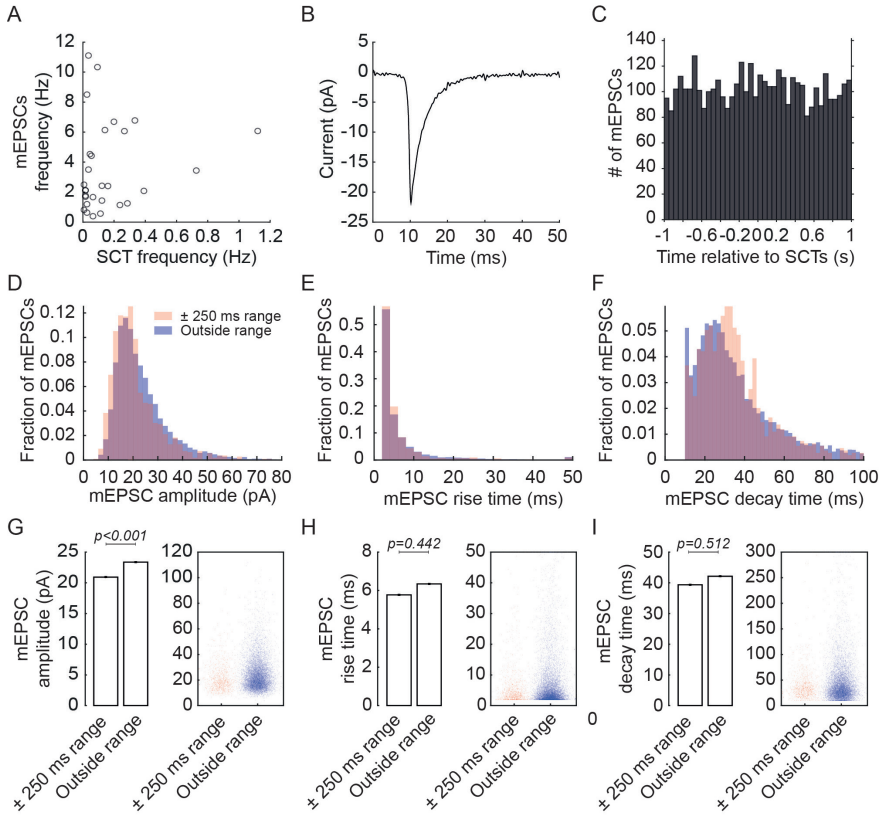

Figure 9. Relative timing and properties of mEPSCs occurring within 1 s before or after SCTs. (**A**) The frequency of SCTs and mEPSCs, determined with simultaneous syGCaMP6f imaging and electrophysiology, are plotted for each of n = 29 autaptic neurons. (**B**) Average mEPSC trace from n = 10260 mEPSCs (**C**) Histogram depicting the number of mEPSCs detected within ± 1 s from each SCT peak for all cells analysed. (**D**) Histogram for mEPSC amplitude, (**E**) mEPSC rise time and (**F**) mEPSC decay time. mEPSCs occurring within ± 250 ms from the SCE peak (pink) showed a similar distribution as mEPSCs occurring outside this time range (blue). (**G-I**) Average amplitude, rise time and decay time ± SEM (left) and data point distribution (right) for mEPSCs occurring within ± 250 ms from the SCT peak (pink; n = 1093) and mEPSCs occurring at other times (outside range, blue; n = 10237). All mEPSCs from 29 cells are included. The statistical significance was tested with Mann-Whitney U test.

We repeated the analysis for all types of SCEs (**Figure 10**). The correlation between SCE and mEPSC overall frequency does not suggest a clear correlation (**Figure 10A**) and, also in this case, the number of mEPSCs was not higher in temporal bins close to SCE peaks (**Figure 10C**). The mEPSCs that co-occurred within ± 250 ms of all SCEs had a slightly lower amplitude than all other mEPSCs (**Figure 10D,G**). In addition, mEPSC rise (**Figure 10E,H**) and decay times (**Figure 10F,I**) were slightly shorter. Altogether these results suggest that mEPSCs are not tightly coupled in time to SCTs or SCEs in the same way as EPSCs are coupled to ECEs.

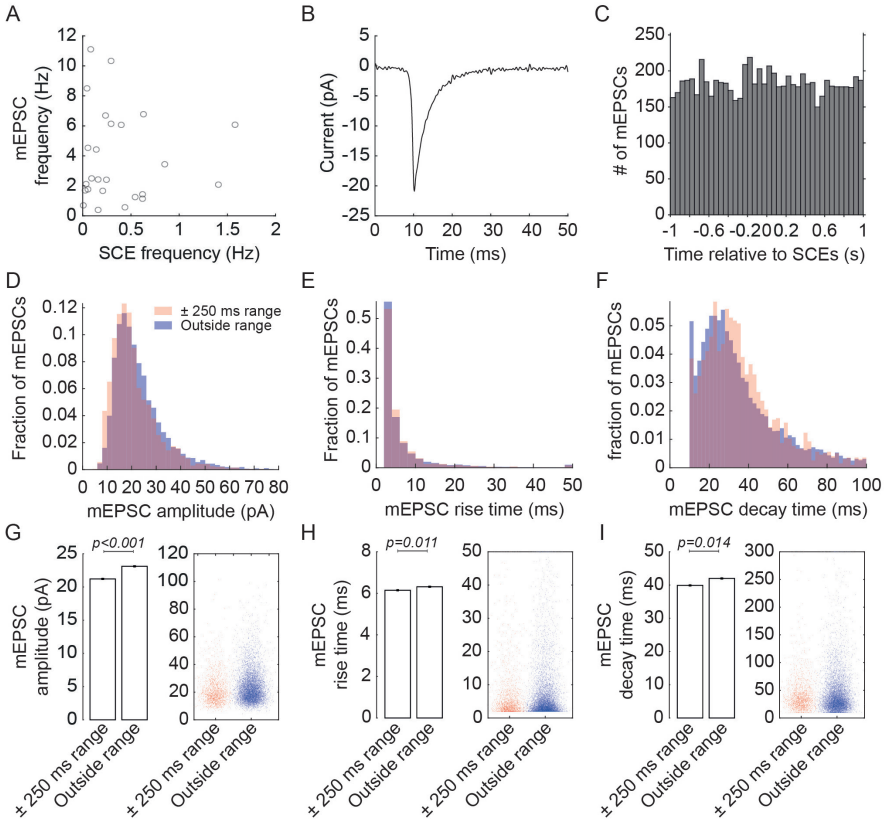

Figure 10. Relative timing and properties of mEPSCs occurring within 1 s before or after all SCEs. Similar analysis as in **Figure 9**, except that all SCEs events were included in the analysis. (**A**) Frequency of all SCEs and mEPSCs from n = 25 autaptic neurons. (**B**) Average mEPSC trace from n = 9450 mEPSCs from the same neurons. (**C**-**I**) Same as in **Figure 9**, showing 1949 mEPSCs occurring within ± 250 ms from the SCE peak time (pink) and 8786 mEPSCs outside this time range (blue).

Spatiotemporal coupling of spontaneous synaptic vesicle fusion to SCEs

As an alternative method to investigate the spatiotemporal co-localization of synaptic fusion events and SCEs, we designed a new probe, called sypHyJRex. To visualise SCEs, we used a new Ca^{2+} indicator, JRex (Molina et al., 2019). To detect spontaneous synaptic fusion events, we used synaptophysin-pHluorin (sypHy) (Granseth et al., 2006). Both pHluorin and JRex were expressed on synaptic vesicles using synaptophysin in such a way that pHluorin was located in the lumen and JRex on the cytoplasmic surface (**Figure 11A**). pHluorin and JRex can be excited with the same wavelength (480 nm) and their emission wavelengths (peaks at respectively 510 and 585 nm) can be separated using a beam splitter as detailed in method section and **Figure 11B**. Similar strategies have been used to simultaneously visualise synaptic fusion events and Ca^{2+} influx but mostly after single and multiple APs (Jackson and Burrone, 2016).

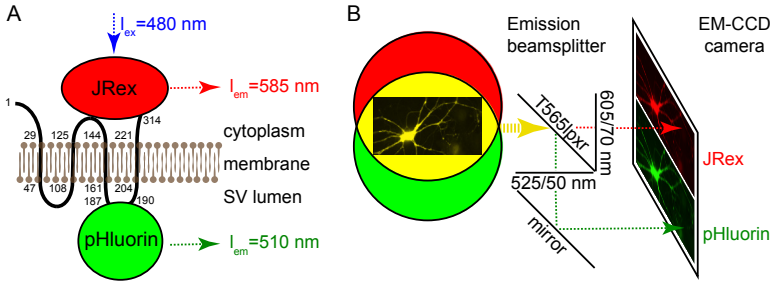

Figure 11. sypHyJRex. (**A**) Cartoon of sypHyJRex structure. pHluorin and JRex were linked respectively on the luminal and cytoplasmic side of synaptic vesicles by inserting them after the 3rd and 4th transmembrane domain of synaptophysin. Numbers indicate amino acids of mouse synaptophysin. pHluorin and JRex are both excited by 480 nm and emit fluorescence at 510 and 585 nm respectively. (**B**) sypHyJRex allows the simultaneous analysis of Ca^{2+} fluctuations and pH changes associated with vesicle secretion events at real time using an emission beam splitter.

To validate if the pHluorin and JRex signals were separately detected, sypHy-JRex was expressed in neurons and imaged during three treatments: acid wash, depolarizing solution and NH_4Cl solution. Acid-wash is known to quench the fluorescence of externalized pHluorin (Sankaranarayanan and Ryan, 2000; Granseth et al., 2006). This treatment reduced pHluorin fluorescence with minor effects on JRex fluorescence (**Figure 12A**).

Second, a depolarizing solution containing 60 mM KCl increases Ca^{2+} influx and triggers synaptic vesicle release (Miesenböck et al., 1998; Akerboom et al., 2013). This increased both pHluorin and JRex fluorescence but with different kinetics (**Figure 12B**): the JRex signal showed a sharp increase immediately followed by a decay (likely due to Ca^{2+} clearance mechanisms), whereas the pHluorin signal was more persistent (likely due to externalization after vesicle fusion). Finally, 50 mM NH_4Cl, which increases the pH of unfused synaptic vesicles but also allows Ca^{2+} to be released into the cytosol (Hui et al., 2015; Lazarenko et al., 2017; Granseth et al., 2006) strongly affected pHluorin fluorescence and also caused a significant signal in the JRex channel (**Figure 12C**). The dual signals induced by NH_4Cl treatment had a similar time dependence and therefore, we

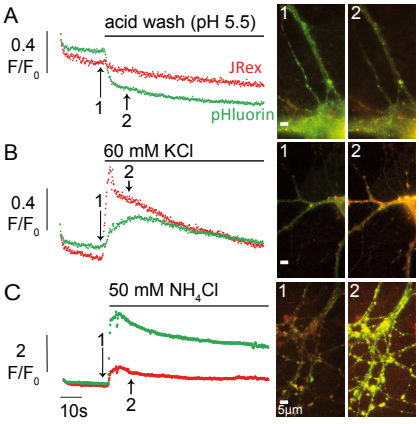

Figure 12. Characterisation of sypHyJRex response. Dual channel emission from JRex (red) and pHluorin (green) with representative image frames taken at the indicated times (arrows) before (1) and after (2) stimulation. Effect of (**A**) acid-wash to quench the fluorescence of externalized pHluorin; (**B**) 60mM KCl to depolarize the neurons, causing Ca^{2+} influx and vesicle secretion, and (**C**) 50mM NH_4Cl, neutralizing the acidic lumen of synaptic vesicles. All treatments except KCl depolarization were done in presence of 1 µM TTX in the extracellular medium.

wanted to further control the optical separation of pH and Ca^{2+} signals by sypHy-JRex. We individually expressed either sypHy or synaptophysin-JRex (syJRex) and recorded both emission channels in response to 60 mM KCl, 50 mM NH_4Cl and acid-wash (**Figure 13A-F**).

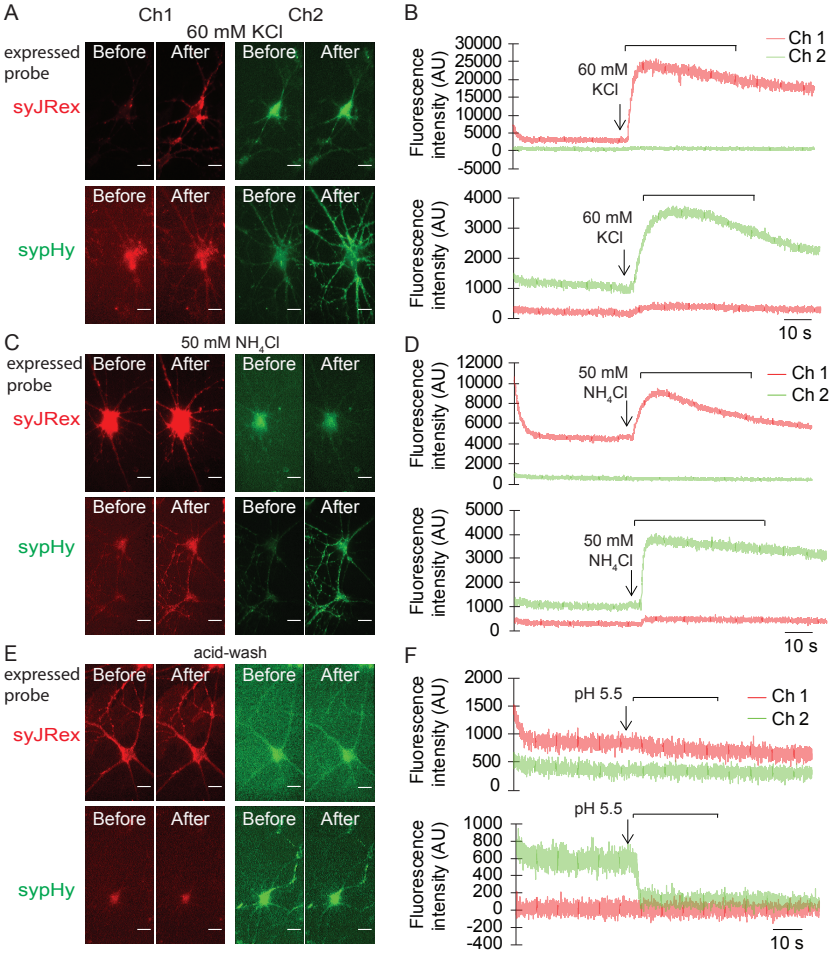

G

	mean amplitude ratio (%)	
	syJRex	sypHy
KCl	2.406 ± 0.037	8.919 ± 0.102
NH_4Cl	n.d.	7.962 ± 0.008
acid-wash	n.d.	2.144 ± 0.371

Figure 13. Optical separation of syJRex and sypHy emission. Time lapse imaging of neurons expressing only syJRex (upper panels; channel Ch1, red) or only sypHy (lower panels; channel Ch2, green). $[Ca^{2+}]_i$ and/or pH changes were induced by perfusion with (**A**-**B**) 60 mM KCl (**C**-**D**) 50 mM NH_4Cl and (**E**-**F**) acid-wash (pH 5.5). (**A**, **C**, **E**) Representative images for Ch1 (left) and Ch2 (right) before and after stimulation; scale bar 20 µm. (**B**, **D**, **F**) Raw intensity values in each emission channel; arrow indicates the time of application. The signal intensity change in both channels was quantitated (lines indicates data points used for quantitation) to calculate the amount of 'bleedthrough' (the percentage of the signal detected in the other channel). (**G**) Table summarizing the percentage of bleedthrough (mean ± SEM) from 2 cells for 60 mM KCl and 50 mM NH_4Cl and 1 cell for acid-wash; n.d. (non-detectable).

Under all conditions tested, the amount of bleedthrough of sypHy fluorescence into the JRex channel was less than 9%. Vice versa, less than 2.5% of the JRex signal was detected in the pHluorin channel (**Figure 13G**).

syJRex and syGCaMP6f

Next, we compared the performance of syJRex with that of syGCaMP6f. To control the optical separation of syJRex and syGCaMP6f emission spectra, neurons expressing a single Ca^{2+} indicator were stimulated with a single AP and a 40 Hz train of 100 APs (**Supplementary Figure 5**). Again, only 2% of the syJRex signal was detected in the syGCaMP6f channel. Vice versa, approximately 10% of the syGCaMP6f signal was detected in the syJRex channel. To compare the amplitude and kinetics of the Ca^{2+} signals reported by each indicator, we co-expressed syJRex and syGCaMP6f in the same autaptic neuron (**Figure 14**). During a 40 Hz train (**Figure 14A-B**), syGCaMP6f presented an approximately 2.1-fold bigger amplitude, a 2.3-fold shorter peak duration (FWHM), a 4.1-fold shorter rise time and a 7.8-fold shorter decay time compared to syJRex (**Figure 14C-F**). The Ca^{2+} response for a single AP showed similar differences (**Figure 14G-I**).

Finally, SCTs were measured while clamping the autaptic neurons at -70 mV. **Figure 14J** shows the average $\Delta F/F_0$ trace of 8 SCTs from 1 cell detected with syJRex and syGCaMP6f. We conclude that syJRex is sensitive enough to detect the Ca^{2+} signal induced by a single AP and can be combined with pHluorin-based probes. Compared to the established probe syGCaMP6f however, syJRex has a 2-fold reduction in signal intensity and slower kinetics.

These properties suggest that live imaging of sypHyJRex can be performed with slower image acquisition speeds, e.g. in the 1–10 Hz range. In hippocampal neurons, live imaging at 4 Hz identified Ca^{2+} signals that immediately preceded a secretory response in the same subcellular locations of neurites expressing sypHyJRex. 13 spontaneous Ca^{2+} events coupled to fusion events were observed in eight cells. Four cells did not show any Ca^{2+} events. Interestingly, we observed SCEs and secretion events that occurred simultaneously in two separate regions of the same neurite of one neuron in presence of TTX (**Figure 15A-C**).

Discussion

SCE characterisation

To elucidate the relation between Ca^{2+} and spontaneous neurotransmission, we recorded SCEs in glutamatergic hippocampal neurons using OGB-1-AM, GCaMP6s/f and the new variant JRex. Various types of Ca^{2+} signals were observed. SCEs consisted of a short-lived Ca^{2+} transient which returned quickly to baseline, here named SCTs (see **Figure 1F, 2K, 6A**). SCTs occurred while clamping autaptic neurons at -70 mV. Their frequency was unaffected by TTX, demonstrating that fast SCTs are AP-independent. The duration of SCTs depended on the indicator used to report them; OGB-1 showed the fastest kinetics with a FWHM of 50 ms.

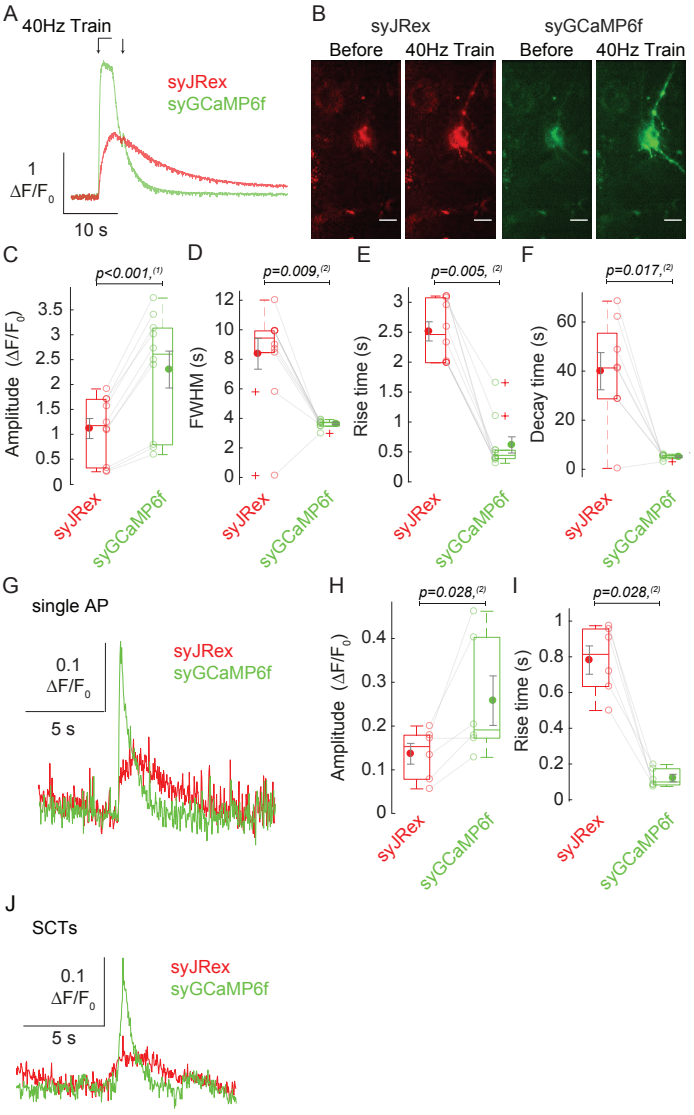

Figure 14. Direct comparison of syJRex and syGCaMP6f sensitivity and kinetics. Ca^{2+} signals reported by syJRex (red) and syGCaMP6f (green), co-expressed in the same neuron during a 40 Hz train (**A**-**F**), a single AP (**G**-**I**) or during SCTs (**J**). (**A**) Average $\Delta F/F_0$ trace induced by a 40 Hz train of 100 APs (n = 10 ROIs, N = 2 cells). The elbow arrow indicates the duration of the 40 Hz train, followed by an additional stimulation with a single AP (arrow). (**B**) Example neuron before and after stimulation; scale bar 20 µm. Quantification of (**C**) $\Delta F/F_0$ amplitude. (**D**) FWHM. (**E**) Rise time. (**F**) Decay time. (**G**) Average $\Delta F/F_0$ trace induced by a single AP (n = 6 ROIs, N = 2 cells). Quantification of (**H**) $\Delta F/F_0$ amplitude. (**I**) FWHM. (**J**) Average $\Delta F/F_0$ trace during SCTs (n = 8 ROIs, N = 1 cell). Statistical significance was tested using (1) Paired samples t-test, (2) Wilcoxon signed-rank test.

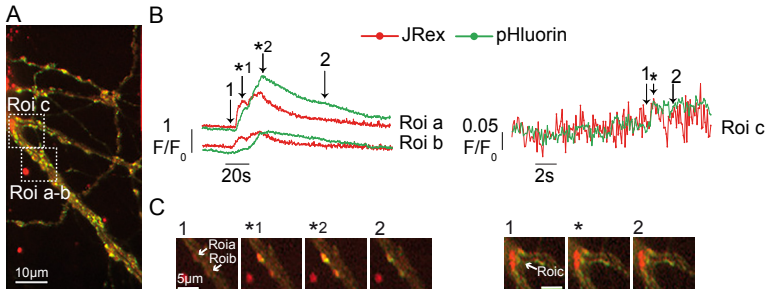

Figure 15. sypHyJRex-based detection of spontaneous fusion events triggered by complex SCEs. (**A**) Example image of sypHyJRex fluorescence in hippocampal neurites. (**B**) sypHyJRex F/F_0 traces, JRex (red) and pHluorin (green) recorded in 1 µM TTX from three different ROIs highlighted in **A** and in detail in **C** show long-lasting SCEs of the complex type. (**C**) Image frames taken before (1), during (*; *1; *2) and after the peaks (2) shown in **B**.

A second category, here named complex SCEs, included multiple other waveforms illustrated in **Supplementary Figure 3B**. It includes Ca^{2+} transients of longer duration, stepwise Ca^{2+} increases, waves and waveforms with multiple peaks.

The average frequency of SCEs in hippocampal neurons ranged from 0–1.5 Hz when including all types of SCEs (**Figure 10A**) or 0–1.1 Hz when excluding complex SCEs (**Figure 9A**). The occurrence of SCEs in the absence of membrane depolarizations is in line with previous studies. Emptage et al. (2001) recorded nicotine-evoked Ca^{2+} transients in a single bouton of OGB-1 labelled, hippocampal-slice cultured neurons in presence of TTX with a frequency of 0.66 events per second (Emptage et al., 2001). Our results (**Figure 7**) suggest that the relation between $[Ca^{2+}]_e$ and mEPSC frequency can partially be explained by a higher global $[Ca^{2+}]_i$. In addition, however, a longer duration of SCTs and a higher frequency of complex SCEs could contribute to this effect. All these changes may be caused by diminished Ca^{2+} clearance by buffers, pumps or exchangers at high extracellular concentrations.

Not all neurons showed SCTs (in our OGB-1-AM experiments 7/8 cells and in our syGCaMP6f experiments 33/40 cells). Similarly in cerebellar Purkinje neurons, some but not all cells show SCTs (Llano et al., 2000). In our experiments, SCTs could possibly remain undetected due to the limited field of view which does not fully cover the neuronal structure, whereas the patch clamp procedure likely detects all mEPSCs. Undersampling of SCTs may also be caused by limited signal-to-noise ratio or a narrow field of depth with high aperture optics.

SCTs were enriched in presynaptic boutons given the colocalization with synapsin and were readily detected by syGCaMP6f, targeted to presynaptic boutons. The idea that SCTs are enriched presynaptically suggests that they may potentially activate presynaptic Ca^{2+} sensors implicated in spontaneous release (Groffen et al., 2010). A subset of 30% of active regions presenting SCTs occurred outside synapses (**Figure 4**). In 2015, Reese et. al detected SCTs in Fluo-4 loaded hip-

pocampal neurons in presence of TTX. In their study, a postsynaptically targeted variant of GCaMP5 detected far fewer events than globally expressed GCaMP5 (Reese and Kavalali, 2015). It is thus possible that both pre- and postsynaptic SCTs occur. The specific presynaptic targeting of GCaMP6f may facilitate future studies towards the contribution of these events.

SyGCaMP6f fluorescence peak was delayed of 150 ms with respect to the EPSC evoked from a single AP. In reality, the Ca^{2+} peak evoked from a single AP is known to occur a fraction of a millisecond before the EPSC (Südhof, 2012). This suggests that syGCaMP6f, despite its fast kinetics compared to other GCaMP derivatives (Chen et al., 2013), still reports the true Ca^{2+} signal with a delay. Compared to syGCaMP6f, syJRex offers slower dynamics with a peak delay of 1.9 s from syGCaMP6f (**Figure 14G**). The signal amplitude is also 2-fold lower. Thus, while sypHyJRex is uniquely capable of reporting Ca^{2+}-secretion coupling by simultaneous dual channel imaging, syGCaMP6f is superior for detecting SCTs in single channel recordings.

Temporal correlation of mEPSC and SCEs

Several studies have addressed the correlation between Ca^{2+} events and SV release (Emptage et al., 2001; Llano et al., 2000; Reese and Kavalali, 2015). Our approach aimed to detect SCE and mEPSC events and compare their timing directly in single neurons. In contrast to EPSCs triggered by ECEs, mEPSCs were not tightly coupled to SCTs. This could indicate that mEPSCs are not triggered by SCTs, or that the delay between the SCT and the mEPSC event is highly variable. We also did not detect a temporal correlation in a wider range of ± 5 s relative to SCTs, or when all types of SCEs were included in the analysis.

Spatial correlation of synaptic vesicle fusion and SCEs

As an alternative approach to investigate Ca^{2+}-secretion coupling mechanisms in spontaneous synaptic release we developed sypHyJRex. syJRex readily detected ECEs induced by a single AP. Unlike GCaMP6, it can be combined with sypHy for simultaneous dual channel imaging. The event shown in **Figure 15** provides proof of principle that presynaptic SCEs can trigger secretory events in absence of membrane depolarization. Importantly, this SCE was of the complex type and showed two distinct peaks in the Ca^{2+} signal, perhaps suggesting an involvement of CICR or other pathways leading to intracellular Ca^{2+} amplification. It remains to be investigated which proportion of spontaneous release events is mediated by this mechanism.

In several neurons (2/8 in experiments with OGB-1 and 3/40 in experiments with syGCaMP6f), a single AP also induced two Ca^{2+} peaks. The first Ca^{2+} peak was fast and global, and it was associated with an EPSC; the second was slower, and propagated as a wave through the neurites. Furthermore, the second Ca^{2+} peak was not accompanied by postsynaptic depolarization. We speculate that the second Ca^{2+} peak originates from a CICR mechanism and may represent Ca^{2+} release from intracellular stores through RyR and IP_3R channels (Verkhratsky and

Shmigol, 1996; Berridge, 1998).

Taken together, we conclude that spontaneous Ca^{2+} events and spontaneous synaptic fusion events can be detected simultaneously and locally with sypHy-JRex; although, we do not know yet if they are strictly correlated and in which percentage they occur. sypHyJRex is, therefore, valuable to perform more detailed analyses of Ca^{2+}-dependent regulation of neurotransmission at the level of single synapses. It would be interesting to identify upstream molecular events which induce SCEs, such as the involvement of various voltage- and ligand-gated Ca^{2+} channels. In addition, the identity of involved Ca^{2+} sensors may deserve attention. The discovery of AP-independent signalling cascades will expedite our understanding of synaptic plasticity and homeostasis, the regulation of neuronal excitability and nervous system development.

Acknowledgements

We thank Robbert Zalm, Jurjen Broeke, Desiree Schut, Frank den Oudsten and Joost Hoetjes for excellent technical assistance and Matthijs Verhage for critically reading the manuscript. This research was funded by the Netherlands Organization for Health Research and Development (ZonMW project 91113022).

Author Contributions

R.M. performed Ca^{2+} imaging with OGB-1, GCaMP6s/f and syGCaMP6f, and electrophysiological recordings. Q.B performed and analysed extracellular Ca^{2+} perfusion experiments. Y.Q. and R.C. developed and characterised jRex-GECO.

A.J.G. developed sypHyJRex, performed dual channel recordings and wrote MATlab code for data analysis. R.L and R.M performed and analysed dual recordings with sypHy, syJRex, syGCaMP6f and sypHyJRex

R.M. and A.J.G. designed the study, interpreted data and wrote the manuscript.

Supplementary figures

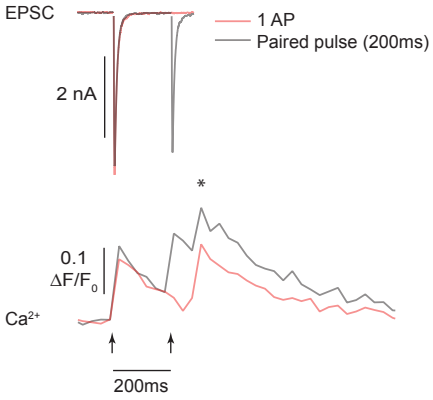

Supplementary figure 1. Double Ca^{2+} response for single AP in 2/8 cells. Representative EPSCs (upper trace) and simultaneously recorded OGB-1 response (lower trace) after stimulation with a single AP (red) or a paired pulse with a 200 ms interval (grey). Recordings are from cell 2 in **Table 1**. The peak times of EPSCs occur simultaneously with Ca^{2+} peaks reported by OGB-1 (arrows). In addition, a third peak (*) was observed with a delay after the first AP.

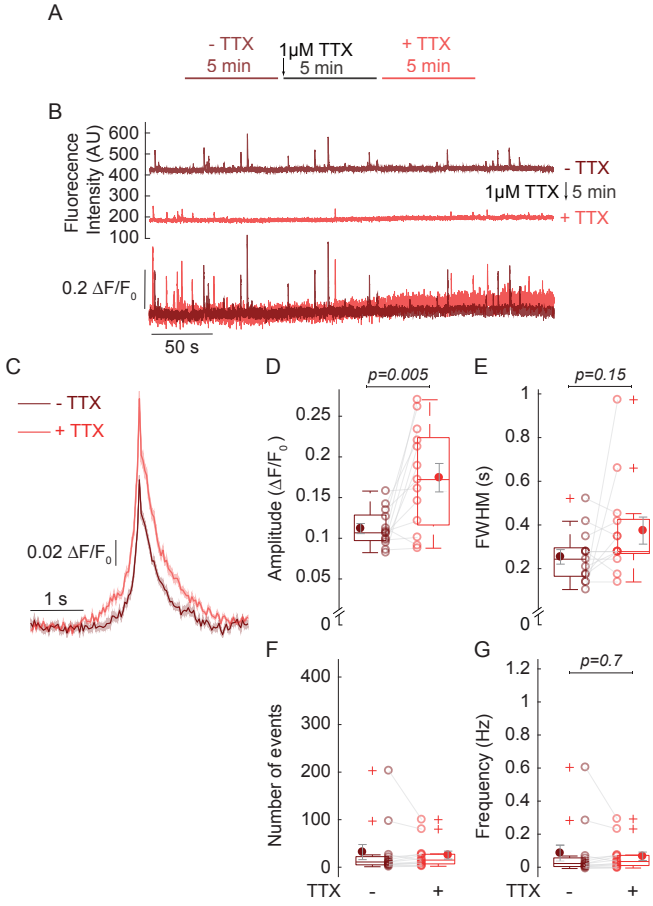

Supplementary Figure 2. Effect of TTX on manually detected Ca^{2+} transients. (**A**) Hippocampal continental neurons expressing GCaMP6f were first imaged 5 min in ACSF, then 1 µM TTX was applied and after 5 min the same neuron was recorded for 5 min. (**B**) Example raw fluorescence traces (upper panel) or $\Delta F/F_0$ traces (lower panel) taken from the same ROI prior to (dark red) and after TTX addition (light red). (**C**) Average $\Delta F/F_0$ trace ± SEM from n = 13 cells. (**D**-**G**) Mean Ca^{2+} transient parameters in absence or presence of TTX. (**D**) Amplitude. (**E**) FWHM. (**F**) Number of events. (**G**) Frequency. Empty dots represent average values per cell; filled dots depict the mean of all cells ± SEM. Central line shows median and statistical outliers are marked by red 'plus' symbols. Statistical significance was tested using Wilcoxon signed-rank test.

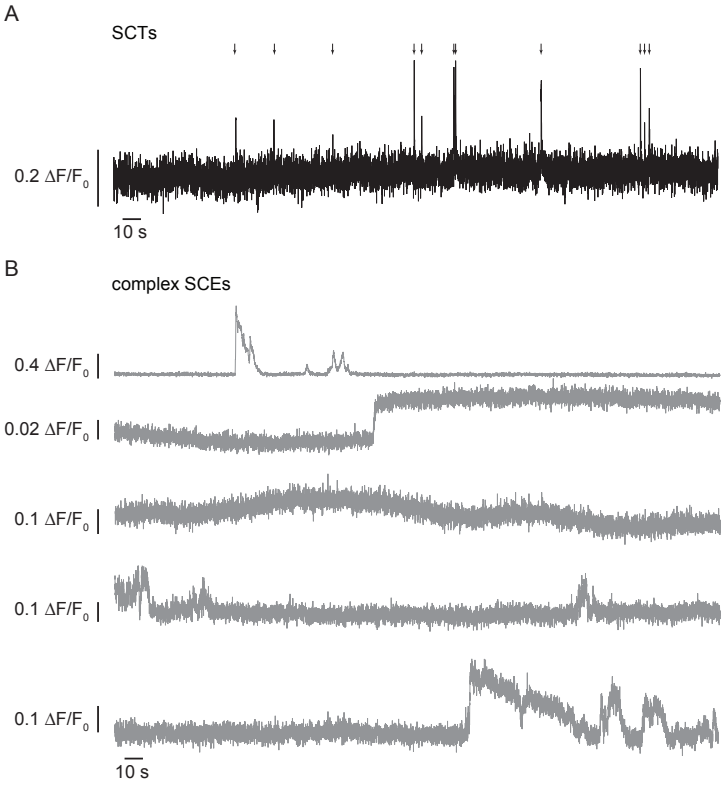

Supplementary Figure 3. Variety of spontaneous Ca^{2+} event kinetics. Representative GCaMP6f $\Delta F/F_0$ traces showing several types of SCEs. (**A**) SCTs, forming the majority of events, were characterised by short-lived Ca^{2+} elevations which returned quickly to baseline. The reproducible kinetics of these events allowed the analysis of kinetic parameters. (**B**) Various other types of Ca^{2+} kinetics were observed, collectively named 'complex SCEs'. When stated, these SCEs were included for frequency quantitation in the following experiments.

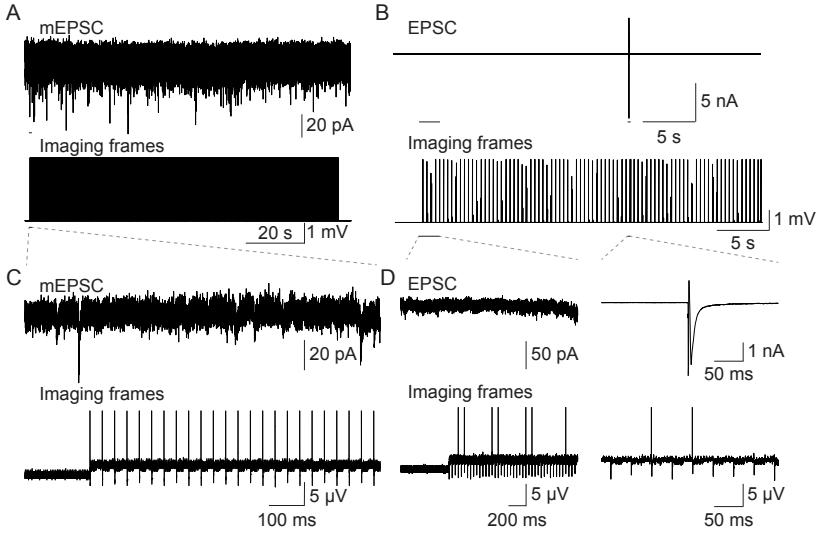

Supplementary Figure 4. Precise synchronization of electrophysiological data sampling and image acquisition. Methodology used to acquire electrophysiological (upper trace) and imaging data (lower trace). (**A**, **C**) The mEPSC recordings were sampled at 250 KHz. (**A**) Example of the whole mEPSC recording (top) and the simultaneously recorded camera shutter signal (bottom). (**C**) Zoomed trace of A at the starting time of the imaging acquisition. The positive peaks were used to determine the precise start and end of each image frame. (**B**, **D**) Evoked stimulations were sampled at 10 KHz due to software limitations. (**B**) Example of a whole electrophysiological recording (top, a single AP stimulation is visible) and the simultaneously recorded camera shutter signal (bottom). (**D**) Zoomed trace of **B** at the starting time of the imaging acquisition (left) and during the stimulation time (right). Positive peaks in the camera shutter signal are too short to be reliably detected, but negative peaks reliably indicate the start and end of each image frame acquisition.

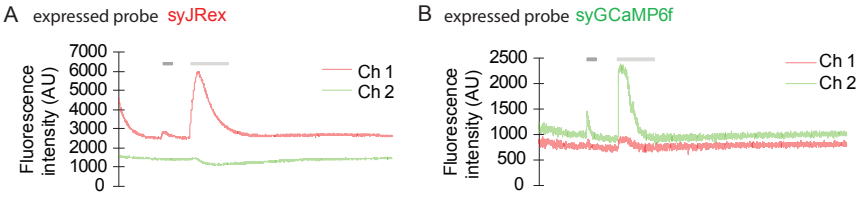

C

mean amplitude ratio (%)			
syJRex		syGCaMP6f	
1st AP	Train	1st AP	Train
n.d	1.947 ± 0.194	8.644 ± 1.146	10.132 ± 0.167

Supplementary Figure 5. Optical separation of syJRex and syGCaMP6f during a single AP and 40Hz train. Time lapse imaging of neurons expressing only (**A**) syJRex (Ch1, red) or (**B**) syGCaMP6f (Ch2, green). Raw emission intensities were recorded in both channels to validate the optical separation of the probes. ECTs were induced by a single AP and a 40 Hz train of 100 APs. Dark grey (AP) and light grey (40 Hz train) bars indicate the data points used for quantitation. (**C**) Summary of the percentage of bleedthrough of each probe in the opposite channel (mean ± SEM from 2 cells; n.d. (non-detectable)).

Supplementary Table 1. Details of statistical tests

Figure 2. GCaMP6s vs GCaMP6f for Ca^{2+} transient detection	Statistical test					Accepted α- significance		Sample
	(1) Independent samples t-test					0.0167		
	(2) Mann-Whitney U test							
Figure references	Parameter	Statistical result	p-value	Statistical test	Effect size (r)	Descriptive (mean ± SEM)		
						GCaMP6s	*GCaMP6f*	
H	Frequency	t(15) = 0.542	p = 0.059	(1)	n.a.	0.11 ± 0.028 Hz	0.09 ± 0.029 Hz	n = 9 cells GCaMP6s, n = 8 GCaMP6f
I	Amplitude	U = 32	p = 0.7	(2)	n.a.	0.064 ± 0.012 $\Delta F/F_0$	0.060 ± 0.006 $\Delta F/F_0$	
J	FWHM	t(15) = 1.817	p = 0.089	(1)	0.40	0.421 ± 0.062 s	0.282 ± 0.041 s	

Figure 3. Effect of TTX on Ca^{2+} transients	Statistical test					accepted α - significance		Sample
	(1) Paired samples t-test					0.01		
	(2) Wilcoxon signed-rank test							
Figure references	Parameter	Statistical result	p-value	Statistical test	Effect size (r)	Descriptive (mean ± SEM)		
						pre-TTX	*post-TTX*	
C	Integrated amplitude	Z = -0.664	p = 0.507	(2)	n.a.	7.67 ± 0.91 $\Delta F/F_0$ x pixels	8.50 ± 0.93 $\Delta F/F_0$ x pixels	n = 13 cells
D	FWHM	t(12) = -0.285	p = 0.780	(1)	n.a.	0.183 ± 0.015 s	0.190 ± 0.019 s	
E	Rise time	t(12) = -0.370	p = 0.718	(1)	n.a.	0.114 ± 0.009 s	0.118 ± 0.011 s	
F	Decay time	t(12) = -0.822	p = 0.427	(1)	n.a.	0.253 ± 0.023 s	0.279 ± 0.030 s	
H	Frequency	Z = -0.525	p = 0.6	(2)	n.a.	0.18 ± 0.09 Hz	0.16 ± 0.06 Hz	

Figure 4. SCTs occur predominantly in synapses

F.r.	Parameter	Statistical result	p-value	Statistical test	Effect size (r)	Descriptive (mean ± SEM)		Sample
						+ synapsin	*- synapsin*	
C	% of Roi active per cell	U = 291	p < 0.001	Mann-Whitney U test	0.59	71.56 ± 4.43%	28.44 ± 4.43%	n = 43 cells, N = 3 independent experiments

Figure 5. Synaptic targeting of GCaMP6f: syGCaMP6f

Fig. ref.	Parameter	Statistical result	p-value	Statistical test	Effect size (r)	Descriptive (mean ± SEM)		Sample
						GCaMP6f	*Sy-GCaMP6f*	
C	VAMPII co-localization Pearson's R value	t(22) = 6.939	p < 0.001	independent samples t-test	0.82	0.49 ± 0.04	0.78 ± 0.02	n = 12 cells GCaMP6f, n = 12 cells sy-GCaMP6f

Figure 6. SCE detection using global GCaMP6f and syGCaMP6f

Figure references	Statistical test					accepted α - significance	Sample
	(1) Paired samples t-test					0.00625	n = 20 cells per group, N = 3 independent experiments
	(2) Wilcoxon signed-rank test						
	Parameter	**Statistical result**	**p-value**	**Statistical test**	**Effect size (r)**	**Descriptive (mean ± SEM)**	
						GCaMP6f	***SyGCaMP6f***
B	Amplitude	t(38) = 1.228	p = 0.227	(1)	n.a.	0.088 ± 0.003 $\Delta F/F_0$	0.094 ± 0.003 $\Delta F/F_0$
C	Area 2D	t(38) = -2.504	p = 0.017	(1)	0.38	150.61 ± 8.77 pixels	121.21 ± 7.80 pixels
D	Integrated amplitude	U = 148	p = 0.160	(2)	n.a.	13.66 ± 1.24 $\Delta F/F_0$ x pixels	11.71 ± 1.09 $\Delta F/F_0$ x pixels
E	FWHM	U = 189	p = 0.766	(2)	n.a.	0.264 ± 0.011 s	0.278 ± 0.022 s
F	Rise time	U = 163	p = 0.317	(2)	n.a.	0.152 ± 0.007 s	0.162 ± 0.009 s
G	Decay time	U = 171	p = 0.433	(2)	n.a.	0.415 ± 0.031 s	0.423 ± 0.028 s
I	SCT frequency	U = 115.500	p = 0.022	(2)	0.36	0.022 ± 0.005 Hz	0.055 ± 0.014 Hz
J	complex SCE frequency	U = 172.500	p = 0.457	(2)	n.a.	0.082 ± 0.015 Hz	0.132 ± 0.030 Hz

Figure 7. $[Ca^{2+}]_e$ affects global $[Ca^{2+}]_i$ SCT decay and SCE frequency

Figure references	Statistical test (within groups comparison)					Accepted α-significance (between-within groups)	Sample
	Pairwise comparison					0.05	n = 11 cells per group
	Parameter	Statistical result	p-value	Statistical test	Effect size (r)	Descriptive and pairwise comparison	
						groups (mean ± SEM)	comparisons	corrected p-value
C	$F_{340/380}$ nm	$X^2(3) = 32$	p = 0.000	Friedman Test	0.862	Cond 1*: 0.28 ± 0.018 (AU)	Cond 1 vs Cond 2	p = 0.416
						Cond 2*: 0.32 ± 0.022 (AU)	Cond 1 vs Cond 3	p = 0.001
						Cond 3*: 0.33 ± 0.026 (AU)	Cond 1 vs Cond 4	p = 0.000
						Cond 4*: 0.33 ± 0.025 (AU)	Cond 2 vs Cond 3	p = 0.285
							Cond 2 vs Cond 4	p = 0.003
							Cond 3 vs Cond 4	p = 0.823

Figure 7. $[Ca^{2+}]_i$ affects global $[Ca^{2+}]_e$ SCT decay and SCE frequency (continue on next page)

Figure references	Statistical test (between groups comparison)					Accepted α-significance		Sample
	(1) One-way repeated measures ANOVA					0.0125		n = 10 cells per group
	(2) Friedman Test							
	(3) One-way repeated measures ANOVA with Greenhouse-Geiser correction							
	Statistical test (within groups comparison)					0.05		
	Pairwise comparison							
	Parameter	**Statistical result**	**p-value**	**Statistical test**	**Effect size (r)**	**Descriptive and pairwise comparison**		
						groups (mean ± SEM)	**comparisons**	**corrected p-value**
E	Frequency	F(1.597,14.342) = 18,281	p = 0.000	(3)	0.738	Cond 1*: 14.510 ± 2.623 Hz	Cond 1 vs Cond 2	p = 0.687
						Cond 2*: 12.305 ± 2.179 Hz	Cond 1 vs Cond 3	p = 0.008
						Cond 3*: 17.117 ± 2.436 Hz	Cond 1 vs Cond 4	p = 0.003
						Cond 4*: 22.012 ± 3.096 Hz	Cond 2 vs Cond 3	p = 0.011
							Cond 2 vs Cond 4	p = 0.007
							Cond 3 vs Cond 4	p = 0.046

Figure 7. $[Ca^{2+}]_e$ affects global $[Ca^{2+}]_i$ SCT decay and SCE frequency (continued from previous page)

F	Amplitude	$X^2(3) = 11.900$	$p = 0.008$	(2)	0.721	Cond 1*: -17.46 ± 9.677 pA	Cond 1 vs Cond 2	p = 1	
						Cond 2*: -15.50 ± 6.834 pA	Cond 1 vs Cond 3	p = 0.599	
						Cond 3*: -14.16 ± 4.813 pA	Cond 1 vs Cond 4	p = 0.011	
						Cond 4*: -12.63 ± 4.307 pA	Cond 2 vs Cond 3	p = 1	
							Cond 2 vs Cond 4	p = 0.116	
							Cond 3 vs Cond 4	p = 0.846	
G	Rise time	$F(1.714,0.588) = 0.472$	$p = 0.604$	(3)	n.a.				
H	Decay time	$F(3,27) = 1.447$	$p = 0.251$	(1)	n.a.				

Figure 7. $[Ca^{2+}]_e$ affects global $[Ca^{2+}]_i$, SCT decay and SCE frequency (continue on next page)

Figure references	Statistical test (between groups comparison)					Accepted α-significance		Sample
	(1) One-way repeated measures ANOVA					0.006		n = 10 cells per group
	(2) Friedman Test							
	(3) One-way repeated measures ANOVA with Greenhouse-Geiser correction							
	Statistical test (within groups comparison)					0.05		
	Pairwise comparison							
	Parameter	**Statistical result**	**p-value**	**Statistical test**	**Effect size (r)**	**Descriptive and pairwise comparison**		
						groups (mean ± SEM)	**comparisons**	**corrected p-value**
J	Frequency	$X^2(3) = 4.758$	p = 0.190	(2)	n.a.			
K	Amplitude	F(3,18) = 0.102	p = 0.958	(1)	n.a.			
L	Area 2D	F(3,18) = 0.100	p = 0.959	(1)	n.a.			
M	Rise time	F(3,18)= 1.193	p = 0.341	(1)	n.a.			

Figure 7. $[Ca^{2+}]_e$ affects global $[Ca^{2+}]_i$, SCT decay and SCE frequency (continued from previous page)

N	Decay Time	F(3, 18) = 4.348	p = 0.018	(1)	0.456	Cond 1*: 0.334 ± 0.068 s	Cond 1 vs Cond 2	p = 0.218
						Cond 2*: 0.367 ± 0.112 s	Cond 1 vs Cond 3	p = 0.033
						Cond 3*: 0.525 ± 0.049 s	Cond 1 vs Cond 4	p = 0.012
						Cond 4*: 0.541 ± 0.048 s	Cond 2 vs Cond 3	p = 0.164
							Cond 2 vs Cond 4	p = 0.186
							Cond 3 vs Cond 4	p = 0.255
O	FWHM	F(3, 18) = 1.132	p = 0.363	(1)	n.a.			
P	Integrated amplitude	F(3, 18) = 0.113	p = 0.951	(1)	n.a.			
Q	Frequency	$X^2(3) = 13.837$	p = 0.03	(2)	0.746	Cond 1*: 0.43 ± 0.391 Hz	Cond 1 vs Cond 2	p = 1
						Cond 2*: 0.45 ± 0.490 Hz	Cond 1 vs Cond 3	p = 0.056
						Cond 3*: 0.90 ± 0.256 Hz	Cond 1 vs Cond 4	p = 0.034
						Cond 4*: 1.15 ± 0.584 Hz	Cond 2 vs Cond 3	p = 0.092
							Cond 2 vs Cond 4	p = 0.056
							Cond 3 vs Cond 4	p = 1
R	Area 2D	$X^2(3) = 1.080$	p = 0.782	(2)	n.a.			

Figure 9. Relative timing and properties of mEPSCs occurring within 1 s before or after SCTs

Fig. ref.	Statistical test				Accepted α- significance		Sample
	Mann-Whitney U test				0.0167		mEPSC n = 1093 within range, n = 10237 outside range; N = 29 cells; 8 independent experiments
	Parameter	Statistical result	p-value	Effect size (r)	Descriptive (mean ± SEM)		
					within ± 250 ms	*Outside ± 250 ms*	
J	Amplitude	U = 4750273	p < 0.001	0.07	-20.92 ± 0.30 pA	-23.37 ± 0.11pA	
K	Rise time	U = 5515474.500	p = 0.442	n.a.	5.77 ± 0.21 ms	6.34 ± 0.08 ms	
L	Decay time	U = 5527152	p = 0.512	n.a.	39.35 ± 0.94 ms	42.12 ± 0.38 ms	

Figure 10. Relative timing and properties of mEPSCs occurring within 1 s before or after all SCEs

Fig. ref.	Statistical test				Accepted α- significance		Sample
	Mann-Whitney U test				0.0125		mEPSC n = 1949 within range, n = 8786 outside range; N = 25 cells; 8 independent experiments
	Parameter	Statistical result	p-value	Effect size (r)	Descriptive (mean ± SEM)		
					within ± 250 ms	*Outside ± 250 ms*	
J	Amplitude	U = 7480875	p < 0.001	0.08	-21.21 ± 0.23 pA	-23.10 ± 0.11 pA	
K	Rise time	U = 8245363	p = 0.011	0.02	6.15 ± 0.16 ms	6.32 ± 0.08 ms	
L	Decay time	U = 8256887	p = 0.014	0.02	39.92 ± 0.68 ms	42.00 ± 0.41 ms	

Figure 14. Direct comparison of syJRex and syGCaMP6f sensitivity and kinetics

Figure references	Statistical test					Accepted α- significance		Sample (N)
	(1) Paired samples t-test					0.0125		N = 2 cells
	(2) Wilcoxon signed-rank test							
	Parameter	**Statistical result**	**p-value**	**Statistical test**	**Effect size (r)**	**Descriptive (mean ± SEM)**		
						syJRex	***syGCaMP6f***	**Sample (n)**
C	Amplitude	t(9) = -6.801	p < 0.001	(1)	0.9	1.11 ± 0.20 $\Delta F/F_0$	2.30 ± 0.37 $\Delta F/F_0$	n = 10 ROIs
D	FWHM	Z = -2.599	p = 0.009	(2)	0.58	8.37 ± 1.04 s	3.62 ± 0.08 s	n = 10 ROIs
E	Rise time	Z = -2.803	p = 0.005	(2)	0.63	2.51 ± 0.16 s	0.61 ± 0.13 s	n = 10 ROIs
F	Decay time	Z = -2.380	p = 0.023	(2)	0.59	39.96 ± 7.57 s	5.10 ± 0.34 s	n = 8 ROIs
Fig. ref.	**Statistical test**					**Accepted α- significance**		**Sample (N)**
	(2) Wilcoxon signed-rank test					0.025		N = 2 cells
	Parameter	**Statistical result**	**p-value**	**Statistical test**	**Effect size (r)**	**Descriptive (mean ± SEM)**		**Sample (n)**
						syJRex	***syGCaMP6f***	n = 6 ROIs
H	Amplitude	Z = -2.201	p = 0.028	(2)	0.635	0.137 ± 0.024 $\Delta F/F_0$	0.258 ± 0.056 $\Delta F/F_0$	
I	Rise time	Z = -2.201	p = 0.028	(2)	0.635	0.781 ± 0.079 s	0.121 ± 0.021 s	

Supplementary Figure 2. Effect of TTX on manually detected SCTs	Figure ref.	Statistical test				Accepted α- significance		Sample
		Wilcoxon signed-rank test				0.0167		n = 13 cells
		Parameter	**Statistical result**	**p-value**	**Effect size (r)**	**Descriptive (mean ± SEM)**		
						pre-TTX	***post-TTX***	
	D	Amplitude	Z = -2.830	p = 0.005	0.55	0.112 ± 0.006 $\Delta F/F_0$	0.174 ± 0.017 $\Delta F/F_0$	
	E	FWHM	Z = -3.180	p = 0.151	n.a.	0.25 ± 0.03 s	0.37 ± 0.06 s	
	G	Frequency	Z = -0.353	p = 0.724	n.a.	0.09 ± 0.04 Hz	0.07 ± 0.02 Hz	